# Recent advances in photoluminescent polymer optical fibers



**Author(s):**
Jakubowski, Konrad; Huang, Chieh-Szu; Boesel, Luciano F.; Hufenus, Rudolf; Heuberger, Manfred

**Publication date:**
2021-06

**Permanent link:**
https://doi.org/10.3929/ethz-b-000475850



**Originally published in:**
Current Opinion in Solid State and Materials Science 25(3), https://doi.org/10.1016/j.cossms.2021.100912

Current Opinion in Solid State and Materials Science 25 (2021) 100912

Contents lists available at ScienceDirect

Current Opinion in Solid State & Materials Science

journal homepage: www.elsevier.com/locate/cossms

# Recent advances in photoluminescent polymer optical fibers

Konrad Jakubowski [a,b], Chieh-Szu Huang [c,d], Luciano F. Boesel [c], Rudolf Hufenus [a,*], Manfred Heuberger [a,b,*]

[a] Empa, Swiss Federal Laboratories for Materials Science and Technology, Laboratory of Advanced Fibers, Lerchenfeldstrasse 5, 9014 St Gallen, Switzerland
[b] Department of Materials, ETH Zurich, 8092 Zurich, Switzerland
[c] Empa, Swiss Federal Laboratories for Materials Science and Technology, Laboratory of Biomimetic Membranes and Textiles, Lerchenfeldstrasse 5, 9014 St Gallen, Switzerland
[d] Laboratory of Inorganic Chemistry, ETH Zurich, 8092 Zurich, Switzerland

ARTICLE INFO

*Keywords:*
Polymer optical fiber
Photoluminescence
Sensing
Light concentration
Polymer processing

ABSTRACT

Polymer optical fibers (POFs) have been utilized in several applications since the late 1950s. Adding photoluminescence (PL) to the fiber considerably widens the optical functionality of POFs and opens new application fields. In recent years, the availability of laboratory-scale production methods with industrialization potential has triggered a surge of new studies and developments in the promising area of PL-POFs. These applications, profiting from the addition of PL to fibers, are identified in this review as: light harvesting, sensing, color illumination, anti-counterfeiting, and random lasing. Progress in these fields is foreseen to generate a need for larger quantities of fibers, therefore large-scale manufacturing and processing methods are becoming more relevant. This review thus provides an overview of the most important developments in this emerging area, together with a description of the key parameters describing PL-POF performance and efficiency.

## 1. Introduction

Fiber-optic transmission of information is historically strongly associated with drawn glass fibers. Before the ground-breaking work done by Kao and Hockam on lowering the losses of waveguides [1], polymers such as polymethyl methacrylate (PMMA) [2] already proved to be interesting competitors to glass, providing unique advantages for some specialized applications. In the mid-sixties, DuPont's first polymer optical fiber (POF), based on PMMA, reached typical attenuation values of 125 dB/km, while glass fibers already featured specifications of around 1 dB/km. At that time, the main driving force was the development of long-range optical communication. As glass-based fiber waveguides clearly outperformed POFs, the latter have not attracted much attention for several decades. Due to a limited speed of optoelectronic couplers, the field of high-speed short-distance links was initially dominated by copper wires. With the development of fast optoelectric couplers and the rise of local digital networks, the interest in POFs triggered new developments in this field [3,4].

While POFs have only been applied selectively in the second half of the 20th century, their lower processing temperatures enabled the addition of photoluminescent (PL) dyes, which revived POF research. The first photoluminescent polymer optical fiber (PL-POF) was realized in 1957 [5] when Reynolds and Condon demonstrated drawn filaments with diameters of 0.5 and 1.0 mm, produced from a plastic scintillator material, for the detection of ionizing radiation. Since then, PL-POFs have been utilized in a variety of scenarios, including sensing, light-harvesting, short-range communication, textile anti-counterfeiting, and local lighting systems. This wide range of application areas is probably the reason for the remarkable variety of proposed PL fiber processing methods, as well as the rather heterogeneous content of respective publications.

This review discusses three groups of PL-POF applications, and covers the advances achieved in the last ten years. A separate section is devoted to PL fiber production methods, highlighting their unique strengths and limitations. An introductory section sheds light on essential differences between standard POFs and PL-POFs by reviewing some fundamental equations governing their optical properties.

* Corresponding authors at: Empa, Swiss Federal Laboratories for Materials Science and Technology, Laboratory of Advanced Fibers, Lerchenfeldstrasse 5, 9014 St Gallen, Switzerland (M. Heuberger).
*E-mail addresses:* rudolf.hufenus@empa.ch (R. Hufenus), manfred.heuberger@empa.ch (M. Heuberger).

https://doi.org/10.1016/j.cossms.2021.100912
Received 2 November 2020; Received in revised form 3 February 2021; Accepted 1 March 2021
Available online 17 March 2021

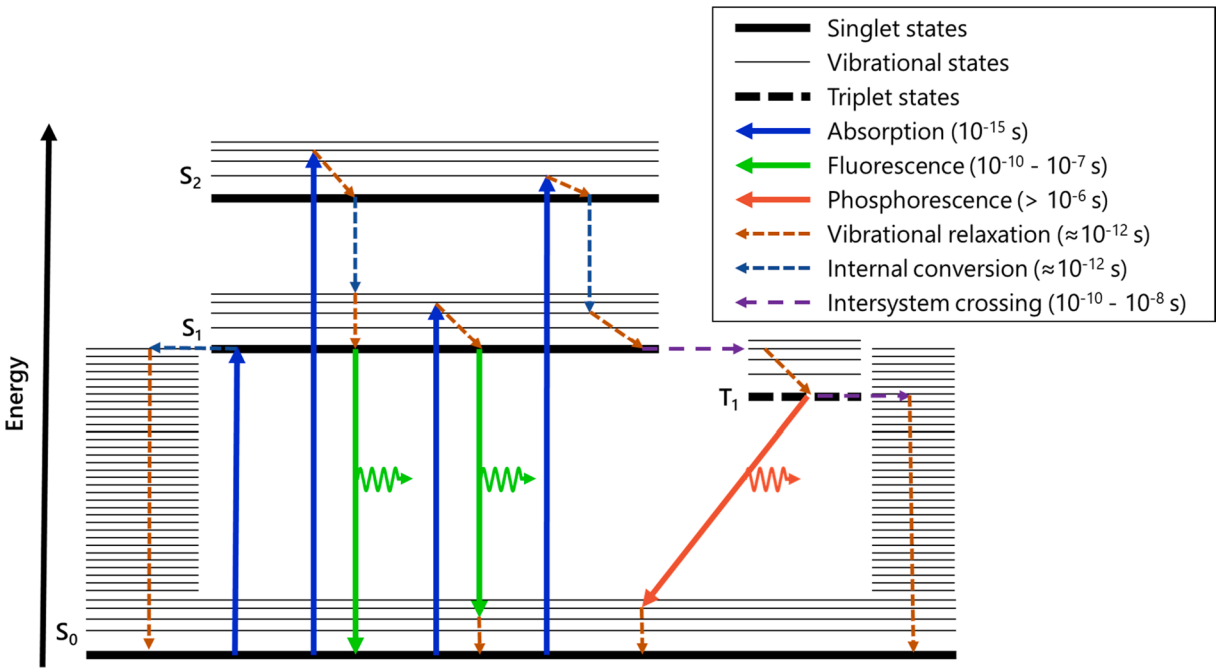


**Fig. 1.** Representation of various processes that take place upon light absorption by a luminophore. Green arrows represent variants of fluorescent emission and the red arrow is a phosphorescent emission, which can be significantly delayed due to the extended lifetime of excited state(s). (For interpretation of the references to color in this figure legend, the reader is referred to the web version of this article.)

## 2. Basics of PL-POFs

Like POFs, PL-POFs utilize the principle of total internal reflection (TIR) [6] for wave guiding: below a critical angle, the light rays traveling within a high refractive index (RI) medium are reflected at the optical interface with a second low-RI material. In the waveguide, light rays may undergo numerous reflections. In the simplest configuration, the low-RI material is air (core-only fiber), with $RI_{air} \approx 1.00$. The best known polymeric example is PMMA, which has $RI_{PMMA} \approx 1.49$ [7]; polycarbonates (PC) have $RI_{PC} \approx 1.58$ [7], polystyrene (PS) $RI_{PS} \approx 1.58$ [7] and cyclo-olefin polymers (COP) $RI_{COP} \approx 1.53$ [8]. In a bi-component core-cladding fiber, the high-RI polymer core is coated with a low-RI cladding, providing both robustness of the optical properties and beneficial mechanical behavior [6,9].

Typically, low-RI polymers are fluorinated polymers, such as polytetrafluoroethylene (PTFE) or terpolymer of tetrafluoroethylene, hexafluoropropylene and vinylidene fluoride (THV), exhibiting RI values as low as 1.34 [10]. In some studies, a low-RI polymer capillary was filled with a high RI liquid, resulting in a liquid-core optical fiber [11–16]. A desired characteristic of fibrous materials is high flexibility, and thus alternative polymers like polydimethylsiloxane (PDMS) have been used [17–19], but upscaling of respective POFs revealed certain application limits: the low RI of PDMS ($RI_{PDMS} \approx 1.41$) [20] implicates a small numerical aperture (NA), which diminishes the fiber's light acceptance cone [21], therefore restricting its capability to capture and transmit luminescent light in PL-POFs [22]. Above list of polymers represents a selection, since many other materials have been investigated as base materials for POFs, and thereby also for PL-POFs [7,23].

The optical acceptance cone defines the highest TIR angle at which the light can enter the core at its end (tip); a higher step difference between the RIs of the two materials leads to higher acceptance angles. POFs do not couple sidelong incoming light. However, the presence of optical imperfections, such as light-scattering impurities or cracks, can couple light in or out of wave guiding modes. While this effect is purposely used in periodic grating couplers or sensor fibers, side-coupling of light is disadvantageous in long-range telecommunication. PL-POFs allow a controlled degree of side-coupling via photoluminescent dye, dispersed within the fiber material. Due to its internal placement, the dye emits much of the light within the fiber's acceptance cone, thus enabling sidewise light collection. PL-POFs are hence prone to perform well in sensing or light collection/distribution over relatively short distance.

Apart from a suitable RI step, the choice of polymeric materials for PL-POFs must include compatibility with the dye and the processing conditions [23,24]:

- The core polymer must be transparent, to facilitate transmission of light.
- The polymers have to enable melt spinning of fibers with good mechanical properties.
- The compatibility of core, cladding and dye material must allow for reproducible co-processing.

Most of the polymers used for PL-POF production are amorphous, since crystalline regions promote light scattering due to a small RI difference between crystalline and amorphous phase [21], especially when present in the core material.

PL-POFs are obtained by doping a waveguiding polymer with a luminophore, i.e. a dye that exhibits photoluminescence, which is a process of light emission that occurs from electronically excited states. Depending on their nature, PL can be divided into two categories: fluorescence and phosphorescence [25]. A common way to illustrate these and other accompanying processes is the Jablonski diagram [26], shown in Fig. 1.

An electron typically exists in a singlet, ground electronic state ($S_0$). A photon of energy equal to or greater than the energy gap between this state and a singlet excited state ($S_i$) interacts with the electron, transferring its energy in a process of absorption. As a result, the electron is excited, usually to one of the higher vibrational levels of an excited state. From there, it undergoes a fast, vibrational relaxation to the lowest energy state of the given excited state. If the energy of the incoming photon is high, and the electron is in an upper excited singlet state $\geq S_2$, it undergoes a fast relaxation to the first excited state ($S_1$) in a process called internal conversion. From there, the electron can either undergo

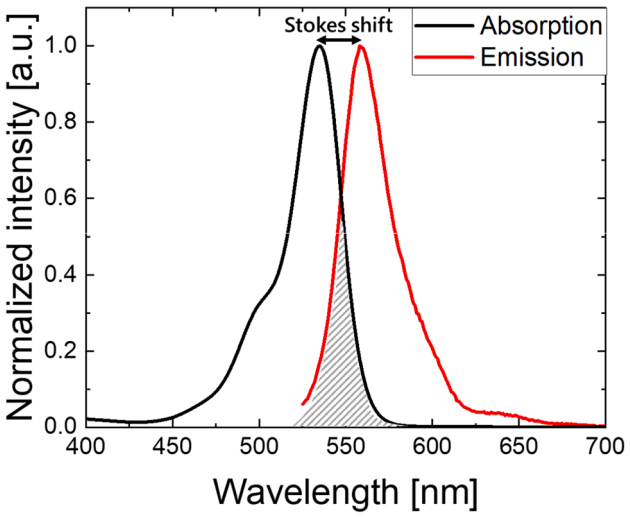


**Fig. 2.** Example of absorption (black curve) and emission (red curve) spectra of a luminescent material, Rhodamine 6G. Stokes shift and the resulting overlap between the two curves are indicated. (For interpretation of the references to color in this figure legend, the reader is referred to the web version of this article.)

another internal conversion to the ground electronic state ($S_0$) without emitting a photon, or it can undergo a process of fluorescence, where a photon is released. The exact energy of the emitted photon is equal to the difference between the energies of the final vibrational level of the ground electronic state and the first excited state. On rare occasions, the electron can undergo a spin conversion from the first singlet excited state to the first triplet excited state in an intersystem crossing process. From there, similar relaxation pathways exist, and the respective photon emission is called phosphorescence. The timescales associated with these phenomena are longer compared to fluorescence – they are called "forbidden transitions", which means that they occur at much lower rates [27].

As a consequence of above processes, three distinct characteristics of photoluminescence arise: Stokes shift, quantum yield (QY) and fluorescence lifetime [28]. The Stokes shift is the difference between energies (or wavelengths) of absorbed and emitted photon. Since the electron undergoes relaxations without emission (vibrational relaxation, internal conversion), the energy of emission is lower than that of the excitation light. When photons are also emitted in the luminescent material's absorption range, absorption and emission spectra can overlap: in waveguides, this results in a prevalent self-absorption problem of the emitted light. Stokes shift and the spectral overlap are schematically illustrated in Fig. 2. QY is a ratio of the number of emitted to absorbed photons. The fluorescence lifetime is the average time, which an electron remains in the excited state. Usually, fluorescent molecules have lifetimes of several nanoseconds.

In condensed matter theory, a quasiparticle called exciton [29–31] is responsible for luminescence. Excitons are electrostatically coupled and overall electrically neutral electron-hole pairs, created when an electron is excited. They can be categorized into two types: Frenkel [32] exciton and Wannier-Mott [33] exciton. A Frenkel exciton has higher binding energy, i.e. energy required to excite the electron, of 0.1–1 eV, a smaller exciton radius, and it appears mainly in organic materials. The most common examples are $\pi$-conjugated organic dyes like rhodamines, coumarins, perylene, and perylene bismides. Especially rhodamine dyes are known to exhibit high QY and high molar-excitation efficiency. However, the small Stokes shift and low photostability of rhodamine limits its use for long-term applications. For coumarin dyes, the Stokes shift is larger, the photostability is better, and the QY is rather high. On the other hand, the emission of coumarin dyes lies in a relatively high energy range, which limits their application for biomaterials and energy harvesting. In general, organic dyes exhibit relatively small Stokes shifts (typically less than 50 nm), as a result of their rather high exciton binding energy. This means that self-absorption is amplified, which limits the practicable dye concentration.

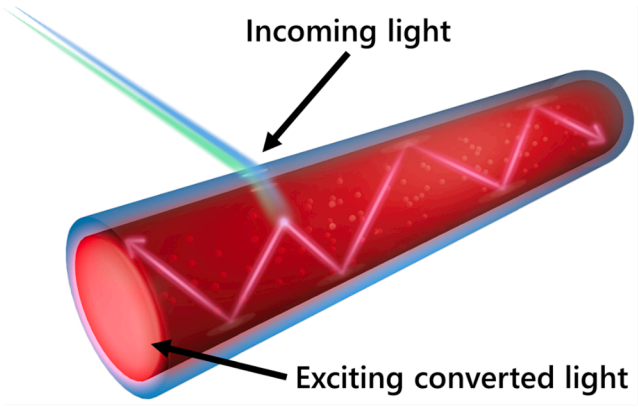


**Fig. 3.** Principle of operation of a PL-POF. External light, approaching the device from the side, is absorbed by dye molecules and undergoes a light-conversion process, during which it is emitted within the fiber acceptance cone. The in-cone portion of the converted light is guided to the end (fiber tip), where it can illuminate a solar cell, a spectrometer, or any other suitable detector. Reproduced with permission from Ref. [41].

The Wannier-Mott exciton occurs in inorganic materials, where the binding energy is lower (in the order of 0.01 eV) and the exciton radius is larger. Among luminescent inorganic materials, ion-based phosphors and semiconductor quantum dots (QDs) are the best-known examples. Among ion-based phosphors, the rare-earth-based organic-inorganic hybrid lanthanide ions (Ln3+) [34] are the most popular. Absorption arises mainly from coordination with organic ligands, and the emission is controlled by the intrinsic f-f transition of lanthanide ions, yielding a large Stokes shift. As for the semiconductor QDs [35] consisting of nanocrystals with several nanometer sizes, the main factors controlling the absorption and emission are the particle size and the intrinsic degeneracy states of the material. Smaller QDs tend to generate blue-shifted emission and absorption due to highly localized states (Dirac distribution)—similar to a dot. The physics of large QDs are more of a three-dimensional nature, therefore bands tend to be continuous and give rise to red-shifted emission and absorption. The nano-material-inherent size-dependence provides a conveniently adjustable range of QD-based luminescence. A more detailed description of photoluminescent processes is beyond the scope of this review, and we thus refer to a respective book by Lakowicz [36].

Different classes of suitable dyes are available, such as organic dyes, nanomaterials, or rare-earth complexes [37–40]. In general, a suitable photoluminescent dye must meet following additional criteria:

- The dye has to disperse well in the selected polymer(s) [23,41], since aggregation of dye molecules can lead to excessive optical absorption and quenching [42].
- The dye absorption/emission spectra should have minimal overlap and should be appropriate for the lighting/detector conditions.
- Processing stability and lifetime of the dye must enable long-term applications.

A schematic representation of the PL-POF's operation principle, illustrating side coupling followed by in-cone emission and wave guiding to the fiber tip, is shown in Fig. 3.

As derived by Muto [43] for glass fibers, the total PL intensity generated by a PL fiber of a given length depends on several parameters:

- The radiant flux of excitation light illuminating the fiber side surface.
- The transmissivity of the fiber side surface.

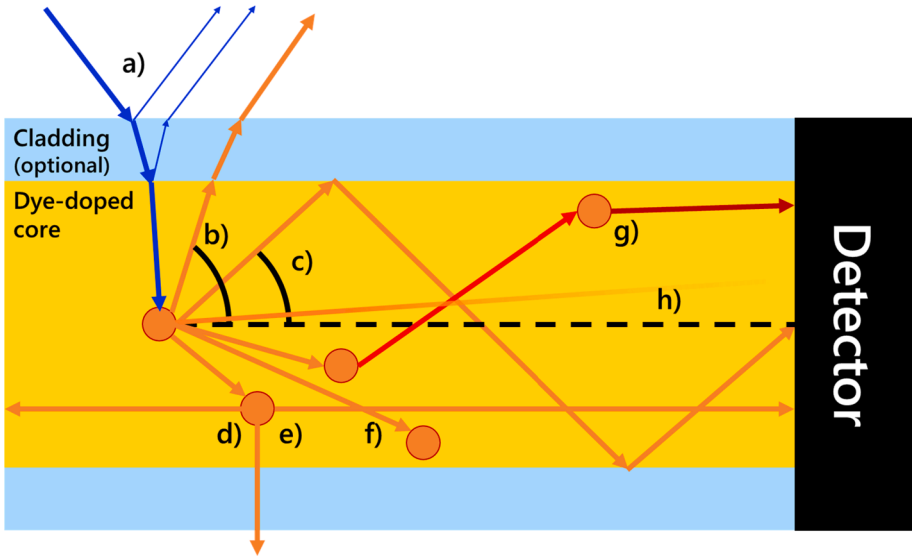


**Fig. 4.** Schematic illustration of the main effects influencing the efficiency of light conversion and propagation in a PL-POF: a) Fresnel reflection from interfaces between two media. b) Loss emission at angles exceeding the trapping angle. c) Emission trapped within PL-POF. d) Self-absorption with re-emission in loss angles, i.e. either opposite to the end device or at angles exceeding the trapping angle. e) Self-absorption with re-emission within the trapping angle. f) Self-absorption without re-emission due to non-unity QY. g) Cascade of self-absorptions with re-emission of less-energetic light due to Stokes efficiency. h) Loss of intensity of emitted light due to background absorption by the polymer or by scattering. For clarity, effects due to multiple Fresnel reflections are not shown.

- The conversion efficiency, relating the radiant flux of the wave guided luminescent light to the flux of excitation light.
- The transmission loss of the PL-POF.

To assess the PL-POF system performance, a property known as "optical conversion efficiency", $\eta_{opt}$, is utilized, which also accounts for propagation losses. It is defined as the photoluminescence fiber tip output power ($P_{out}$) divided by the power of side surface illumination ($P_{in}$), and can be written as a product [44,45]:

$$\eta_{opt} = \frac{P_{out}}{P_{in}} = (1-R) \times \eta_{abs} \times \eta_{Stokes} \times \eta_{Q} \times \eta_{trapping} \times \eta_{transport} \times \eta_{self} \quad (1)$$

where $R$ is the reflection coefficient from the surface of the fiber, $\eta_{abs}$ is the dye absorption efficiency of the incoming side illumination, $\eta_{Stokes}$ is the energy loss factor related to the Stokes shift, $\eta_{Q}$ is the QY of the dye, $\eta_{trapping}$ is the trapping efficiency (viz. acceptance cone) of light re-emitted into the waveguide, $\eta_{transport}$ is the efficiency of the light propagation and $\eta_{self}$ is the efficiency factor relating to repeated self-absorption of converted light by other dye molecules. The factors in Equation (1) depend on the properties of dye and polymers used, as well as on the geometry of the luminescent solar concentrator; their qualitative understanding is crucial for optimizing device efficiency. Noteworthy, all of the aforementioned parameters are wavelength-dependent.

The term $(1-R)$ represents the fraction of the incident light reflected from the PL-POF sidelong surface, where R is the reflectivity of the outer optical interface. The respective equations for s- and p-polarized light are:

$$R_S = \left| \frac{n_1 \cos\theta_i - n_2 \cos\theta_t}{n_1 \cos\theta_i + n_2 \cos\theta_t} \right|^2 \quad (2\prime)$$

$$R_p = \left| \frac{n_1 \cos\theta_t - n_2 \cos\theta_i}{n_1 \cos\theta_t + n_2 \cos\theta_i} \right|^2 \quad (2\prime\prime)$$

Here, $n_1$ is the refractive index of the medium surrounding the device, $n_2$ is the refractive index of the PL-POF outer material, and $\theta_i$ and $\theta_t$ are angles of incidence and transmission, respectively. For unpolarized light (e.g. sunlight), the effective reflection coefficient is the arithmetic mean of above two terms:

$$R_{eff} = \frac{R_S + R_P}{2} \quad (3)$$

The factor $\eta_{abs}$ represents the spectrum-integral absorption efficiency of the dye for a given incident illumination spectrum [46]:

$$\eta_{abs} = \frac{\int_{300}^{E_G^{dye}} S(\lambda) A(\lambda) d\lambda}{\int_{300}^{\infty} S(\lambda) d\lambda} \quad (4)$$

where $S(\lambda)$ is the incident photon flux spectrum, $E_G^{Lum}$ is the bandgap of the luminophore in nm, and $A(\lambda)$ is the absorption spectrum of the luminophore, according to the Beer-Lambert law [47]:

$$A(\lambda) = 1 - 10^{-\alpha(\lambda) \cdot c \cdot l} \quad (5)$$

Here, $\alpha(\lambda)$ is the wavelength-dependent absorption coefficient, $l$ is the effective light propagation length, and $c$ is the concentration of the photoluminescent dye.

Furthermore, $\eta_{Stokes}$ in Equation (1) is the energy down-shift factor connecting to the longer wavelength of emitted light in luminescence. Mathematically, this is the ratio between the averaged (i.e. spectrum center-of-gravity) energy of emitted photons and the averaged energy of absorbed photons in the down-conversion process. Therefore, $\eta_{Stokes}$ is normally smaller than one:

$$\eta_{Stokes} = \frac{\bar{\lambda}_{absorbed}}{\bar{\lambda}_{emitted}} < 1 \quad (6)$$

where $\bar{\lambda}$ are the averaged wavelengths (i.e. reciprocal energies). Note that for some dyes, so-called up-conversion can occur when multiple adsorbed photons contribute to one emitted photon. In such a case, $\eta_{Stokes}$ can be larger than one [48]. These dyes have considerably lower QY [49], which may limit their usefulness in certain applications, such as light concentration.

The next factor, $\eta_{Q}$, considers QY of the dye, which is the probability of emitting a photon upon absorbing one [50]:

$$\eta_{Q} = \frac{\#photons\ \ emitted}{\#photons\ \ absorbed} \quad (7)$$

$\eta_{transport}$ describes the efficiency of light propagation within the waveguide. Propagating light can be absorbed by the polymer base material. Furthermore, light can be scattered out by crystalline regions or other inclusions [51,52]. Likewise, path deviations can occur due to optical interface imperfections or local fiber bending [6].

$\eta_{trapping}$ quantifies the fraction of luminescent light that is trapped by

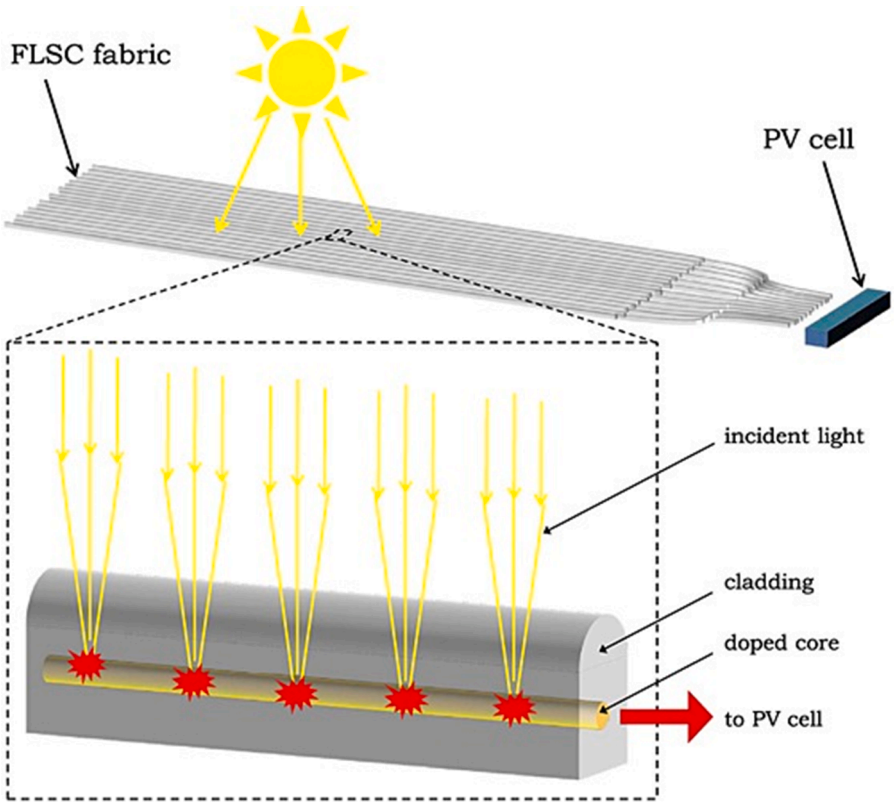


**Fig. 5.** Schematics of a fiber-based light concentrator setup. A textile structure of PL-POFs covers a large area, collecting sunlight via side illumination and light-conversion; radiative energy is guided towards a small-sized PV cell at the end. Reproduced with permission from Ref. [45].

the acceptance cone of the wave guide. Mathematically, the acceptance cone in a cylindrical geometry can be expressed with the following equation [53]:

$$\eta_{trapping} = \sqrt{1 - \left(\frac{n_{cladding}}{n_{core}}\right)^2} \tag{8}$$

where $n_{cl}$ and $n_{co}$ are the refractive indices of cladding and core, respectively. Equation (8) is identical to the often-cited equation for trapping efficiency in planar waveguides of rectangular cross-section. In contrast to the latter, as shown by McIntosh et al. [22], light emitted from molecules dispersed in a cylindrical fiber experiences a range of trapping efficiencies which depends on the emitting molecule's distance from the optical interface defining the acceptance cone.

Finally, in Equation (1), $\eta_{self}$ considers the losses in the carried power due to repeated self-absorption of the emitted light by other luminescent centers. In analogy to Equation (4), a self-absorption probability can be expressed as follows:

$$P_{re-absorption} = \frac{\int_{300}^{E_G^{dye}} S_{dye}(\lambda)A(\lambda)d\lambda}{\int_{300}^{\infty} S_{dye}(\lambda)d\lambda} \tag{9}$$

where $S_{dye}(\lambda)$ is the emission spectrum of the dye. A more detailed study of self-absorption can be found in the supplementary information of [54,55]. Once the light undergoes a self-absorption process, it is susceptible to all the aforementioned loss mechanisms [50,56] (apart from Fresnel reflections). It has been shown [57,58] that luminescent light of wavelength in the dye's absorption range, propagating inside a PL-POF, is attenuated orders of magnitude stronger than light outside of this range.

To conclude this section, Fig. 4 illustrates schematically various processes that impact light traveling within PL-POFs. The end device can be a detector, a PV cell, or something else that fits the intended application.

## 3. PL-POFs used as solar light concentrators

Currently, the best performing photovoltaic (PV) cells are reported to reach efficiencies around 40% under ideal laboratory conditions, while established PV cells just exceed 20% [59]. The conventional strategy to increase solar energy production is to increase the area covered by PV cells, at a proportional increase of costs [60]. Luminescent solar concentrators (LSCs) can enhance energy production via a different approach, as first proposed in the 1970s [61–64]. Today, the work on LSCs is largely dominated by planar slab waveguide approaches [65–67]. Less attention is given to PL-POFs, although they come with a number of benefits, such as light-weight, flexibility, as well as the availability of established large scale manufacturing and processing techniques [68]. For LSC applications, a PL-POF has to be optimized to deliver maximal optical power near the maximum efficient wavelength of the PV cell. The PV enhancement with/without LSC can be described with a LSC-gain factor $F$ [69,70], which is defined as the ratio of power generated by a solar cell with LSC ($P_{LSC}$), to the power generated by the cell alone ($P_{cell}$):

$$F = \frac{P_{LSC}}{P_{cell}} = \eta_{opt} \times G \times \eta_{cell} \tag{10}$$

where $\eta_{opt}$ is the optical conversion efficiency of the LSC (see Equation (1) for PL-POF), and $\eta_{cell}$ is the efficiency of the PV cell. $G$ is a geometrical gain factor pertaining to the concentration of light from the larger collector area to the smaller PV area; it is analogous to an improvement of the photon capture area, calculated as the ratio between total light-harvesting area of the LSC ($A_{collection}$) and the PV cell area ($A_{output}$):

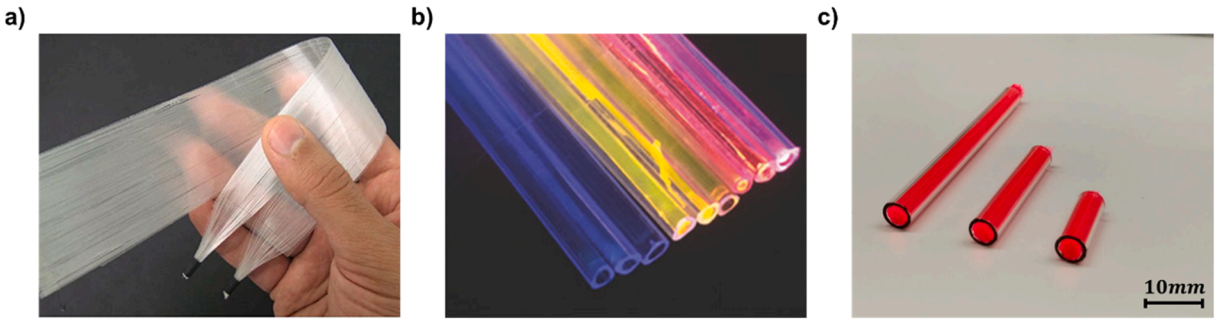


**Fig. 6.** a) A solar-light harvesting textile based on shape-optimized fiber LSCs. Reproduced with permission from Ref. [45]. b) Bundle of liquid-core triangular fibers with three different dyes under UV light illumination. Reproduced with permission from Ref. [85]. c) Photography of PL-POF bundles within PMMA tube. Reproduced with permission from Ref. [41].

$$G = A_{collection}/A_{output} \tag{11}$$

A schematic illustration of an LSC based on PL-POFs is presented in Fig. 5, where the importance of a large G-factor is obvious. Fig. 6**a** depicts the respective light harvesting textile.

The approach utilizing luminescent concentrators has two additional advantages over passive systems like mirrors or lenses:

- The down-conversion of light renders LSCs more suitable for PV cells, since panels interact best with a light of energy close to their band-gap [44,71].
- Luminescent conversion erases the information about the angle of incidence of the excitation light by the process of re-emission, thus alleviating the limitation of passive concentrators [72,73], which collect light only within the limits of the etendue [74–77]. In luminescent solar concentrators, where incoming light is converted by the dye and emitted within a waveguide, the etendue is redefined, enabling a large field of view.

Work on PL-POFs includes different aspects of optimization of the LSC gain factor *F*. Wu et al. [55] performed a detailed analysis of self-absorption utilizing a rare-earth complex with large Stokes shift to obtain PMMA-based fibers that are quasi free of self-absorption. Inman et al. [78] presented hollow-core PMMA-fibers doped with QDs emitting in the near-infrared region, claiming that such structures allow for better excitation absorption and lower self-absorption, since light is propagating in the air while maintaining a similarly high G-factor.

Banaei et al. [79] designed a fibrous LSC, based on a dye-doped COP core and a custom-shaped COP cladding. The shape of the cladding was optimized to unidirectionally focus the incoming excitation radiation onto the core, thus enhancing the overall performance. Another structure of a shape-optimized fiber-based LSC consisted of an undoped COP cladding surrounding a luminescent-doped PC core [45]. This study also demonstrated the beneficial influence of a reflective side surface of the fiber LSC, placed opposite to the light source; a respective enhancement was already predicted by Edelenbosch et al. [80] with ray-tracing methods. The approach with specially shaped fibers is rather complex, since it requires careful manual assembly for correct orientation of individual fibers.

Parola et al. [81] showed that, by co-doping a fiber with two different luminophores, namely a combination of organic dyes and metal-organic material, it is possible to expand the harvesting spectral range by increasing the overall width of the PL-POF absorption spectrum and thus create a more efficient LSC. By monitoring power production over extended periods, they also found that after the initial, fast emission intensity decay, the performance of their best device reached a plateau at 64% of the starting value when exceeding 600 h of illumination. Interestingly, fibers doped with a single organic dye showed no significant initial decrease over the first several hours of exposure, as has been observed for double-doped fibers [82,83]. The group further explored the double-doping approach, showing the impact of the fiber diameter on the LSC performance: when the output power is relevant, fibers should have larger diameter; on the other hand, when the output irradiance is of importance, smaller fibers are advantageous [84].

Correia et al. [69] presented two original geometries of fiber LSCs: fibers coated with a luminescent layer, and hollow-core fibers filled with an active luminescent fluid. The second approach proved to have higher trapping efficiency, mainly due to the higher refractive index step. The latter design also proved to be optically more robust, since the polymeric sheath surrounding the core acted as protective layer, preventing mechanical damage in the waveguiding element. The group later expanded the idea towards hollow-core triangular fibers, filled with the same active material, and bundled together into a planar structure (Fig. 6b) [85].

A theoretical investigation by Videira et al. [86] demonstrated that cylindrical arrays of LSCs outperform planar LSC waveguides, thanks to multiple reflections, lensing, and tailored shadowing between adjacent fibers. LSC fiber bundles were also used by Galatus et al. [87] to extend the battery lifetime of a remote sensor device. Similar bundles, based on an up-scalable melt-spinning production approach, were studied by Jakubowski et al. [41]. This study focused on eliminating the solar midday peak, which relates to the dependence of PV power generation from the incidence angle $\alpha$ of solar light. When considering fiber bundle LSCs, Equation (1), describing optical conversion efficiency, can be written as:

$$\eta_{opt}(\alpha) = \frac{P_{out}(\alpha)}{P_{in}(\alpha)} = \frac{I_{out}(\alpha) \times A_{out}}{I_{in} \times A_{collection}(\alpha)} \tag{12}$$

where $P_{out}(\alpha)$ and $P_{in}(\alpha)$ are effective output and input powers, $I_{out}(\alpha)$ and $I_{in}$ are output and input flux intensities, and $A_{out}$ and $A_{collection}(\alpha)$ are effective emitting and collecting areas, respectively. The mentioned angular dependency stems from an effective change of $A_{collection}$: at shallow angles, the incoming light is received by a larger projected area of the vertically positioned LSC bundle. Fig. 6c shows the fiber bundles prepared in this study. Recently, Besida et al. [88] presented a fiber LSC with photonic crystal cladding, which enables excitation light to enter the fiber, while preventing emitted light to escape at angles exceeding the TIR requirements.

Luminescent fibers were also investigated as omnidirectional collectors in free-space optical communication [89]. Like stratified LSCs, they allow collecting electromagnetic signals from a large area and room angle, using arrays of fibers, thus improving the minimal signal-to-noise ratio (SNR). Peyronel et al. [90] studied commercial fibers mounted in a detector setup with an active area of 126 $cm^2$, achieving data rates up to 2.1 Gb/s with a safety conform emitter intensity. Along similar lines, Riaz et al. [91,92] investigated PL-POFs as a way to improve Wi-Fi networks for indoor applications. They demonstrated an increase of data capacity of a communication channel by augmenting its SNR, achieved by enlarging the light collection area.

**Table 1**
Overview of PL-POFs for electromagnetic radiation harvesting. The active system refers to the luminophore or a combination of luminophores used in the study. In the case of concentration-dependent surveys for one fiber geometry, only the best results are shown.

| Fiber material | Active dye system | Maximal $\eta_{opt}$ (LSCs), purpose (signal concentrators) | Ref. |
|---|---|---|---|
| PMMA | $Eu(TTA)_3Phen$ metal-organic complex | Not provided | [55] |
| | PbS quantum dots | 7.5% (hollow fibers)<br>4.0% (solid core fibers) | [78] |
| | Combination of dyes, including organic perylene derivatives, coumarines and metal-organic complexes | 0.23% | [81] |
| | Combination of dyes, including organic perylene derivatives, coumarines and metal-organic complexes | 0.29% | [84] |
| | Rhodamine 6G-doped organic-inorganic hybrids | 8.0% (hollow fibers)<br>0.08% (coated fibers) | [69] |
| | $Eu^{3+}$-doped organic-inorganic hybrids | 2.3% (hollow fibers)<br>0.01% (coated fibers) | [69] |
| | Rhodamine 6G organic dye | 1.52% (hollow, triangular fibers)<br>0.33% (hollow fibers)<br>0.18% (coated fibers) | [85] |
| | $Eu^{3+}$ complex | 1.14%(hollow, triangular fibers)<br>0.02% (hollow fibers)<br>0.06% (coated fibers) | [85] |
| PS | Unspecified amber dye | Unspecified | [87] |
| | Unspecified dye, peak emission around 500 nm | Increasing the effective area and field-of-view of a free-space optical communication signal receiver | [90] |
| COP | DCM organic dye | 5.7% | [79] |
| PC (core), COP (sheath) | Unspecified luminophore | 7.2% | [45] |
| COP (core), THV (sheath) | Lumogen Red organic dye | From2.0%to15%(angle-dependent) | [41] |
| Unspecified | Unspecified | Unspecified optical efficiency | [88] |
| | Unspecified, green-emitting dye | Increasing the effective area and field-of-view of a free-space optical communication signal receiver | [91,92] |

Photoluminescence introduces an upper limitation to maximum rates in data communication, due to a finite lifetime of the excited state, which is in the range of several nanoseconds [25]. Considering current data-transfer standards, which require communication frequencies of several GHz, the aforementioned PL property implicates a statistical signal delay. The choice of appropriate dyes for PL-POFs, exhibiting short lifetimes of the excited state, is thus crucial in achieving improved detectors for higher optical frequencies; in consequence, the development of respectively improved dyes will be an important future task [93].

Fiber light concentrators come with certain form-factor advantages over comparable planar devices. While planar waveguides can already be found in commercial applications [94–96] and have recognized future potential [97], additional progress is still required to bring fibers to a similar level. The required improvement must focus on large-scale processing of transparent polymers with new dyes, which are characterized by prolonged outdoor stability and enhanced light-conversion. Long-term stability has been recognized as a factor limiting the outdoor application of LSCs prepared with organic light-converting dyes. A regular replacement of the devices would be required when their performance deteriorates due to dye degradation [98–100]. However, Slooff et al. [101] have shown that the outdoor stability of LSC plates can be improved by a proper selection of the host polymer, mainly by choosing high purity. By utilizing distilled PMMA, as compared to commercial plexiglass containing unreacted monomers, dye degradation could be significantly reduced. Another approach to improve outdoor stability is to replace organic dyes with inorganic QDs – some of which are recognized to be more stable under constant illumination conditions [102]. An additional advantage of QDs is their tunable Stokes shift, allowing for reduced self-absorption of the emitted light [103–106], which is a significant loss mechanism, as outlined in Section 2. Using QDs to overcome issues prevalent in LSCs, is gaining more and more attention in the scientific community, and further information can be found in several comprehensive reviews [38,107,108]. While changing the type of luminophore helps to lower the self-absorption, it does never completely remove it, and thus another method to compensate for this effect has been proposed by Krumer et al. [56,104] – it has been demonstrated, that increased luminophore concentration counteracts self-absorption in planar LSCs, an approach which could also be explored in PL-POFs in the future.

Table 1 summarizes the PL-POFs for light harvesting, with emphasis on material composition and optical performance. The conversion efficiency listed for fiber LSCs is relatively low, which is caused by the usage of either un-optimized material composition and fiber geometries, or systems without appropriate connection between concentrator and PV cell. Tackling those challenges by optimizing the design of a fiber concentrator, and by creating an optically improved connection, will eventually allow to achieve higher efficiencies.

## 4. PL-POFs for sensing applications

POFs are already widely used as signal guides or transducers in sensor applications [109–111]. Transduction includes converting one type of energy into another, ideally a human readable one. PL-POFs can readily act as transducers, excited by an incoming radiation of choice (e.g. visible light, high-energy radiation, sub-atomic particles, etc.), and changing emission characteristics depending on sensed quantities like external force or presence of an analyte [112]. Therefore, an added value of PL-POFs is the simple excitation that often waives the need for a specially engineered light source. From a historical perspective, the first application of PL-POF sensors was the detection of ionizing radiation.

While detection of ionizing radiation was demonstrated with undoped fibers through the means of Cherenkov radiation [113] or radiation-induced attenuation [114], fibers doped with special molecules are described as scintillating fibers. Such scintillating fibers (e.g. provided by Kuraray or Saint-Gobain Crystals) consist of a high-RI, dye-doped core (e.g. PS), surrounded by a low-RI primary cladding (e.g. PMMA), both coaxially surrounded by a low-RI secondary cladding (e.g. fluorinated PMMA). Different types of scintillating dyes can be added to the polymer matrix [115], many of which are treated as a trade secret. Currently, the main focus in this field is directed to the design and assembly of scintillating detectors. Here, the aim is to record the flying path of elementary particles to determine their energy and identity. In one proposed setup, fiber layers are stacked into ribbons; when a particle passes through such an assembly, it excites scintillation, and the produced light is then received by a space-resolved detection system, providing information about the particle path [111,116–120]. In an alternative design, optimized for calorimetry, the energy of passing particles can be determined [121,122]. This latter design is similar to the above tracker ribbons, but individual fibers (or layers of fibers) are separated by dense absorbers, which repeatedly absorb a known portion of the energy of the passing particles. The resulting emission of secondary electrons with progressively decreasing energy is then used to

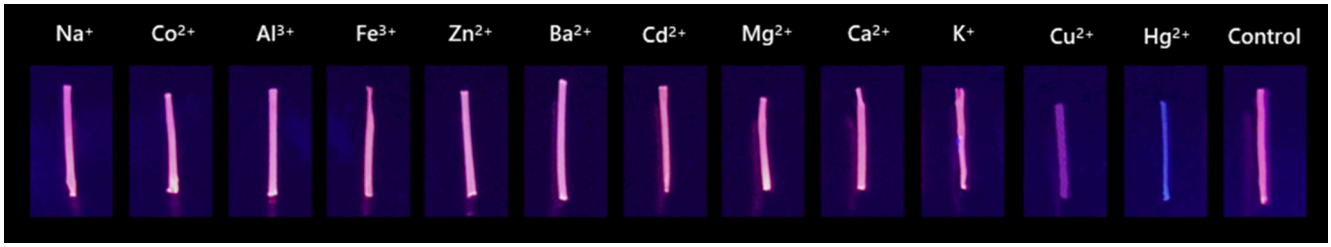


**Fig. 7.** Demonstration of colorimetric detection of Cu2+ and Hg2+ ions using PL-POFs that change their emission color and intensity when in contact with specific ions. Reproduced with permission from Ref. [144].

deduce the energy of the passing particle. This second prominent application of scintillating POFs is optimized for medical applications, including in-vivo dosimetry [123] and radiology [124]. As was investigated by Laguesse and Bourdinaud [125], PL-POFs can be subject to accelerated aging when irradiated by high-energy (e.g. ionizing) excitation light; both, aging of the polymer and the dye can occur [126,127]. For more detailed information about the recent progress in scintillating POFs, we refer to the respective book chapter by Stajanca [128].

PL-POFs are also used to detect less energetic or non-ionizing radiation, such as ultraviolet (UV) or visible radiation. Here, the external excitation light passes through the PL-POF transducer, inducing luminescence, and creating re-emission of proportional intensity. Fitzpatrick et al. [129] demonstrated the feasibility of using PL-POFs, consisting of a doped cladding and a waveguiding core, to monitor the intensity of high-power UV lamps. Miluski et al. [130], also utilizing a doped cladding, studied a UV-A (315–400 nm) fiber sensor. The same group demonstrated UV-light detection by a uniformly doped PMMA fiber, directly analyzing both luminescence intensity and intensity ratios of the luminescent emission peaks [131]. Szolga et al. [132] used PL-POFs to detect plasma emission from switching arcs in electrical distribution boards; the flexibility of those fibers allowed optimal board integration. Mahidhar et al. [133] applied fluorescent fibers to monitor discharges in liquid nitrogen, which occur in electrical power applications of high-temperature superconductors. This method gave similar results as the conventional ultrahigh-frequency method, indicating the yet unexplored potential of PL-POFs in this field.

A common sensing principle is based on the fact that PL-POF waveguiding is affected by the geometry of optics, such as bending angle, pressure, elongation, or simply the distance between illumination position and fiber tip. Recently, PL-POFs were used as bending sensors [134,135], since bending leads to local leakage of light, when a portion of the guided light no longer obeys TIR. Along the same line, PL-POFs were also employed as proximity sensors [136]. By varying the position of the side-illumination along the PL-POF's longitudinal axis, the emission intensity changes as a function of varying attenuation. Proper calibration assumed, such propagation losses can be used to calculate how far from the fiber tip the excitation process took place. This approach may aid in facilitating precise alignment [137,138].

For pressure sensing, Kamimura et al. [139] utilized fibers containing two different luminescent dyes, one in the core and one in the cladding: when pressure is applied on the fiber, light emitted by the dye in the core leaks to the cladding, where it is specifically absorbed by the other luminophore. Recently, Guo et al. [140] demonstrated stretchable PL-POFs based on PDMS to detect strain: upon elongation, the light travels a longer path within the fiber and is accordingly more absorbed. As shown by Jakubowski et al. [58], strain sensing can also be performed using POFs with a liquid glycerol core doped with luminophore. Here, elongation was detected by measuring the shift of the luminescence peak caused by the dye self-absorption; the use of liquid-core fibers, featuring a semi-crystalline sheath, enabled reversible and irreversible strain detection of up to 10% and 350%, respectively.

The effect of fluorescent quenching at elevated temperatures can be used as a measure of temperature [36], which was also demonstrated experimentally utilizing fibers [141]. The aforementioned group (Guo et al.) likewise studied temperature sensing with stretchable fibers, resulting in discriminating multi-parameter sensing devices for strain and temperature [140,142]. Here, lanthanide-based up-converting nanoparticles, which exhibit distinctively temperature-sensitive luminescence peaks at 545 nm and 525 nm, promise a robust measure of temperature by calculating the intensity ratio between the two, i.e. $I_{545\ nm}/I_{525\ nm}$.

Chemical sensing with a luminophore-doped POF core has been demonstrated by Farago et al. [143], based on the interaction of a selective analyte with the luminophore (i.e. via fluorescent quenching), where the cladding was partially removed to expose the core. In a case study, this fiber was put in contact with saliva, and certain fluorescent wavelengths were absorbed when blood was present in the solution. He et al. [144] presented a fluorescent fiber-based sensing platform to detect $Cu^{2+}$ and $Hg^{2+}$ ions, where the fluorescence is quenched by the ions. Here, the quenching rate can be calibrated to the concentration of the respective ionic species (Fig. 7). Inglev et al. [145] demonstrated localized oxygen sensing based upon undoped POFs, where the luminescent behavior is introduced by splicing two such fibers together using a special mixture containing phosphorescent dye. In presence of oxygen, the luminescent intensity of those splices decreases, giving an indication of its concentration.

A noteworthy family of chemical PL sensors is represented in the form of nanofiber-based photosensitive membranes. Although they have no waveguiding properties like PL-POFs, these devices offer a fiber platform for analytes detection, based on changes in their PL characteristics, as illustrated by the following examples. Wang et al. [146] prepared nanofiber membranes populated with well-tuned perovskite QDs, used to detect Rhodamine 6G dye in aqueous and ethanol solutions down to 0.01 ppm. Since the absorption of rhodamine optimally overlaps with the emission of the QDs, amplified energy transfer between the two can occur, greatly enhancing the emission of Rhodamine 6G for detection. Hu et al. [147] demonstrated a reversible and photo-stable HCl gas sensor based on porphyrin-doped porous nanofibers, where the analyte acts as a fluorescence quenching agent, with quenching kinetics proportional to the HCl concentration. Shu et al. [148] prepared polyethylene terephthalate (PET) nanofiber membranes, which change their luminescence in oil vapor; when oil is adsorbed on the surface of the membrane, it absorbs the excitation light, which otherwise would excite the luminescent nanofibers, hence it reduces the emission intensity. The group also demonstrated a possibility to de-oil the structure and reset the measuring device. Hsu et al. [149] presented a fiber membrane tailored to detect ammonia down to a concentration of 110 ppb, with the potential of re-using it up to six times after washing. Petropoulou et al. [150] demonstrated another approach to ammonia gas sensing, based on natural cellulose nanofibers. Thanks to the large surface-to-volume ratio of the substrate, a concentration of up to 1.2% of ammonia could be detected in aquatic solutions, with good linearity

**Table 2**
Overview of PL-POFs for sensing. The active system refers to the luminophore or a combination of luminophores used in the study.

| Fiber material | Active system | Sensing mechanism | Ref. |
|---|---|---|---|
| PMMA | Europium complex | Detection of UV light based on excitation dose variation | [131] |
| | Coumarin 540A (in the core), Rhodamine 6G (in the cladding) | Pressure sensing by changes in the energy transfer between the two dyes | [139] |
| | Rhodamine B | Temperature sensing via fluorescence quenching | [141] |
| | Platinum Octaethylporphyrin | Oxygen concentration sensing via phosphorescence quenching | [145] |
| PMMA (core), polyurethane (sheath) | Tinopal | Detection of UV-A radiation based on excitation dose variation | [130] |
| PS | Unspecified green dye | Partial discharge in liquid nitrogen detection based on excitation dose variation | [133] |
| | Unspecified dye, peak emission around 450 nm. | Bending angle determination by the variation in PL intensity | [134,135] |
| | Unspecified dye, peak emission around 660 nm. | Illumination-position determination by the variation in PL intensity | [136] |
| | Unspecified dye, peak emission around 540 nm. | Illumination-position determination by the variation in PL intensity | [137] |
| | Unspecified dye, peak emission around 645 nm. | | |
| | Unspecified dye, peak emission around 450 nm. | Detection of blood in saliva by emitted light absorption | [143] |
| | $CsPbBr_3$ quantum dots | Rhodamine 6G detection in aqueous media via energy transfer | [146] |
| | 5,10,15,20-tetraphenylporphyrin | HCl detection by fluorescence quenching by the analyte | [147] |
| PS (core), vinyl acetate (sheath) | Unspecified dye | X and gamma radiation detection based on excitation dose variation | [125] |
| PS (core), fluorinated PMMA (sheath) | Unspecified dye | X and gamma radiation detection based on excitation dose variation | [125] |
| Glycerol (core), THV (sheath) | Rhodamine 6G | Strain sensing by measuring the emission peak shift caused by self-absorption of the dye | [58] |
| PDMS | Lanthanide-based upconverting nanoparticles | Strain sensing based on the increased attenuation upon elongation. Temperature sensing based on changing the emission intensity of the luminescent system | [140,142] |
| PET | p-Methylbenzoic acid terbium complex | Oil detection by covering the luminescent nanofibers, thus preventing excitation | [148] |
| Alginate | Red-emitting gold nanoclusters | Detection of heavy ions based on fluorescence quenching | [144] |
| Poly(vinylidene fluoride-co-hexafluoropropene) | Carbon dots with fluorescein | Repeatable ammonia detection down to 110 ppb. | [149] |
| Cellulose acetate | Core-shell $\gamma$-$Fe_2O_3$/$SiO_2$/Rhodamine B nanoparticles | Ammonia detection via fluorescence quenching by the analyte | [150] |
| Unspecified | Unspecified red and green phosphors | Detection of the UV-light based on excitation dose variation | [129] |
| | Unspecified red dye | Arc and flame detection based on excitation dose variation | [132] |
| | Unspecified yellow dye | Illumination-position determination by the variation in PL intensity | [138] |
| | Cyano-substituted vinylacridine derivatives | Aromatic amines and acid vapors detection via fluorescence quenching by the analytes | [151] |

over a wide range of pH, until optical quenching became too strong. Xue et al. [151] utilized gel nanofibers as host material to enable quenching of aggregation-induced emission, and applied them for the detection of aromatic amines and acid vapors, with detection limits of 1.3 $\mu g/m^3$ and 2.3 $mg/m^3$, respectively.

A summary of the aforementioned PL-POFs proposed for sensing applications is given in Table 2, with emphasis on material composition and sensing mechanism.

## 5. PL-POFs for special applications

Although PL-POFs mainly attracted attention as light harvesters and sensing probes, recently several other noteworthy applications emerged.

He et al. [144] described a novel type of PL-POFs to be used as fluorescent anti-counterfeiting elements when stitched into cotton textiles; these fibers provide means of identification under UV-light illumination. A similar approach, based on weaving PL-POFs into fabrics, was presented by Ding et al. [18], where stretchable fibers can be utilized as aesthetically appealing decoration elements. Recently, Erdman et al. [152] prepared luminescent cellulose fibers, which can be incorporated into paper to produce documents and banknotes that impede counterfeiting.

In the field of optical fiber lightening technology, Miluski et al. [153] demonstrated the suitability of PL-POFs, employing double-doped fibers that emit spectrally broad, visible light upon UV-excitation. Cennamo et al. [154] used red and blue PL-POFs as portable ambient light sources to excite a surface plasmon resonance (SPR) in biosensing, which successfully lowered cost and complexity of the setup, rendering powered halogen lamps unnecessary. Lin et al. [155] presented nanofiber membranes as stretchable, moisture-resistant covers for blue LEDs, thus extending the lifetime of white light emitters under ambient air conditions. A rare approach using phosphorescence was presented by Luo et al. [156], where the PL-POFs exhibited a persistent afterglow after excitation stopped.

As already demonstrated two decades ago [157], PL-POFs can also function as so-called “random lasers” [158–160], where the required energy feedback mechanism is provided by random scattering at particles embedded in the PL-POF matrix. This feedback is in contrast to conventional Fabry-Perot cavities [161] or distributed feedback lasers [162,163]. However, with high enough pump energy (called “pump threshold”), lasing can be obtained, which provides speckle-free laser illumination for imaging [164–166], as shown in Fig. 8.

Table 3 highlights some recent advances in the use of PL-POFs as anti-counterfeiting agents, illumination systems, random lasers, or optical communication signal detectors.

## 6. PL-POF production methods

There are several standard POF production methods [167,168] that can be adopted for the preparation of photoluminescent fibers, simply by adding luminophore at a suitable stage of production. Table 4 summarizes the production techniques proposed by aforementioned publications.

While the first two methods listed in Table 4 are discontinuous, the others can operate in a (semi-)continuous mode, provided that the material is constantly supplied.

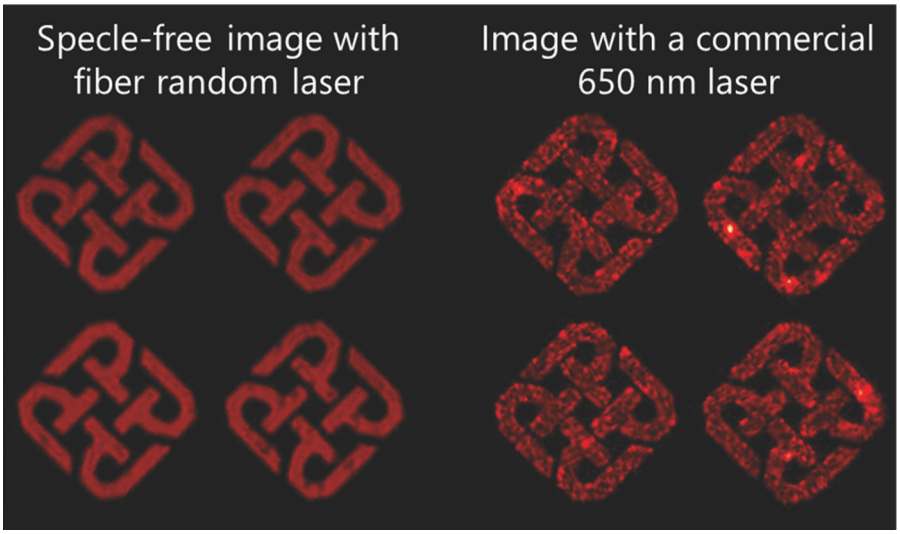


**Fig. 8.** Optical images of the Hong Kong Polytechnic University logo mask, back-illuminated by PL-POF based laser and 650 nm commercial laser. Reproduced with permission from Ref. [145].

**Table 3**
Overview of PL-POFs proposed for anti-counterfeiting, as light sources or random lasers. The active system refers to the luminophore or a combination of luminophores used in the study.

| Fiber material | Active system | Application | Ref. |
|---|---|---|---|
| Alginate | Red-emitting gold nanoclusters. | Anit-counterfeiting, allowing a simple way to identify textiles. | [144] |
| Polypropylene | $Sr_2MgSi_2O_7:Eu^{2+},Dy^{3+}$ phosphor | Fibers exhibiting luminescent afterglow | [156] |
| PDMS | Three tetraphenylethylene (TPE)-derivatives, with blue, green, and yellow emission characteristics. | Decorative yarns with potential to assist in anti-counterfeiting | [18] |
| Cellulose | Star-shaped poly((9-carbazolyl)methylthiirane) | Document and banknote anti-counterfeiting | [152] |
| PMMA | Perylene and Rhodamine 6G | White light (ca. 3350 K) illuminator under 405 nm excitation. | [153] |
| PS | Unspecified dyes, peak emission around 660 nm and 450–500 nm. | Light source (alternative to halogen lamps) for plasmonic sensing. | [154] |
| Poly(styrene–butadienestyrene) | Cesium lead halide perovskite nanocrystals | Luminescent, water-resistant covers for LEDs | [155] |
| Poly(methyl methacrylate-co-benzyl methacrylate) | Pyrromethene 597 and gold nanoparticles | Random lasing arising from the waveguide-plasmon-scattering. | [158] |
| | Polyhedral oligomeric silsesquioxanes (POSS) nanoparticles and Pyrromethene 597 | Random lasing | [159] |
| | Fe3O4/SiO2 nanoparticles and Pyrromethene 597 | Random lasing | [159] |
| Poly(methylmethacrylate-co-benzylmethacrylate-co-methacrylisobutyl) | Pyrromethene 597 | Random lasing | [159] |
| | Rh640 perchlorate-dye with titanium oxide nanoparticles | Random lasing | [160] |

### 6.1. Polymerization and curing

In POF production via polymerization, a mixture containing the host matrix as a monomer and a curing initiator is injected into a silicon mold. To manufacture PL-POFs, the educts can readily be doped with luminescent dyes prior to curing. During the process, the host polymer chains are cross-linked, resulting in a stable fiber structure (Fig. 9). Depending on the base material, curing can be initiated by UV light or temperature. The resulting fiber is detached from the mold either by breaking the latter, or by applying mechanical force (e.g. water stream). In a second step, the core-only fiber can be coated with a low-RI cladding material in a dip-coating process, creating a core-cladding POF.

This process of polymerization and curing is rather time-consuming, and the maximum length of the mold is limited, both because of manufacturing constraints and restricted feasibility to detach the fiber. Although this method is not industrially scalable, it is popular at the academic laboratory scale [17,18,169–175], since it does not require specialized machinery.

Polymerization can be one of the techniques used to produce preforms for the thermal drawing process described in Section 6.4.

**Table 4**
Overview of PL-POF production methods proposed.

| Method | Ref. |
|---|---|
| Polymerization and curing | [78,131,140,142] |
| Thermal drawing | [45,55,69,79,81,82,84,85,88,130,131,139,141,153,158,160] |
| Wet-spinning | [18,144,152] |
| Electrospinning and gelation | [146,149,147,148,150,155,151] |
| Co-extrusion and melt-spinning | [41,58,156] |

### 6.2. Thermal drawing

Thermal drawing has been widely used in the optical fiber industry to produce fiber-like waveguides from glass and polymers alike. Thermal drawing is actually the most common way to produce photoluminescent fibers (Table 4). It owes its popularity to a large flexibility in cross sectional composition and the possibility to produce very long uniform fibers at drawing rates around 0.5 m/s [168]. Thermal drawing is a batch-process and essentially consists of two steps (Fig. 10**a**):

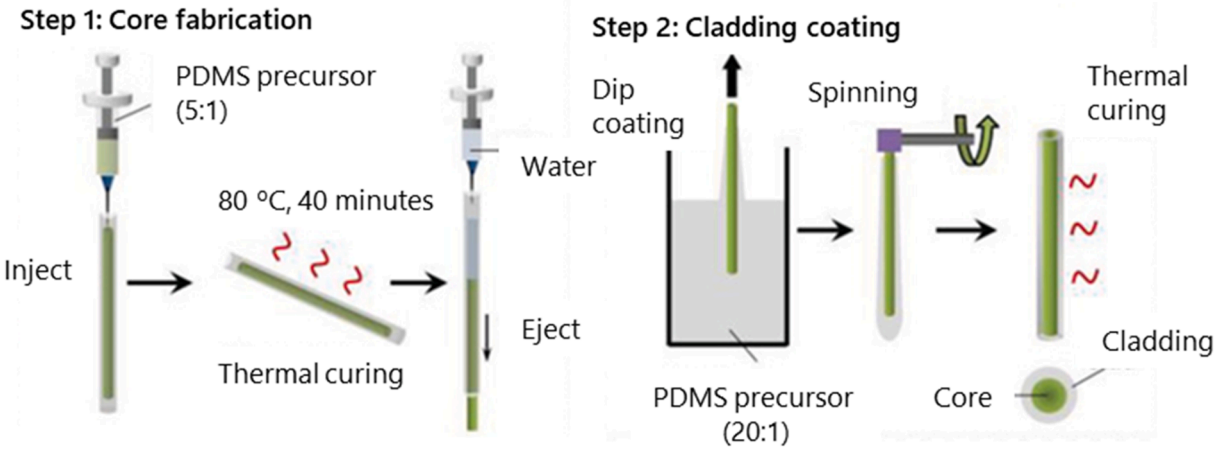


**Fig. 9.** Schematic representation of the polymerization and curing process to produce POFs. A polymer precursor with a reaction initiator is inserted into a mold, which is removed after the reaction is complete. In a second step, a low-RI coating is applied via dip-coating. Reproduced with permission from Ref. [128].

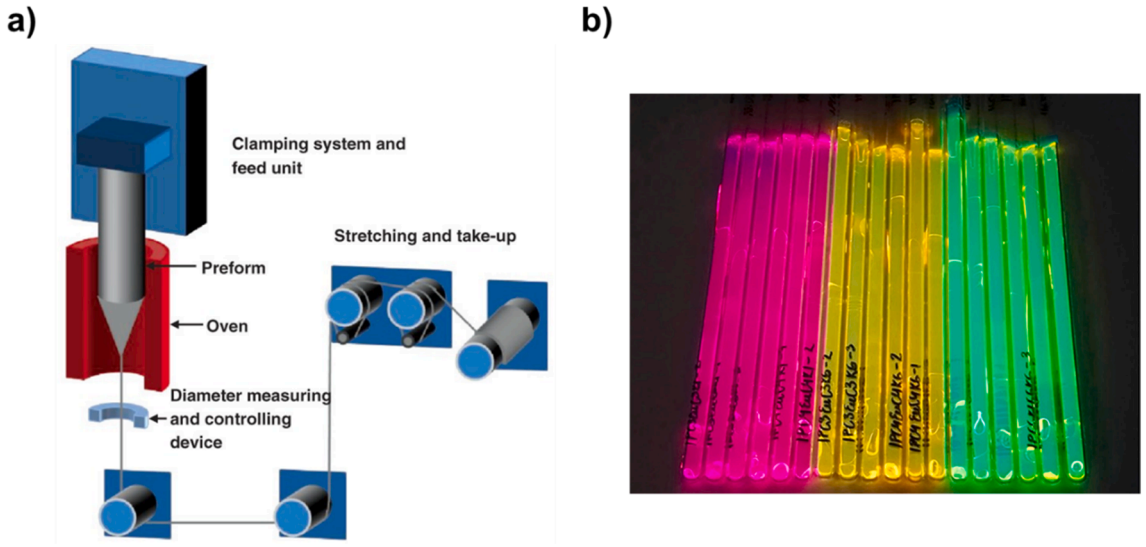


**Fig. 10.** a) Schematic of a drawing process: a preform is clamped in the feed unit, and its bottom is heated above the base material's glass transition temperature. The tapering tip of the preform is finally pulled and stretched by godets to form a fiber. Reproduced with permission from Ref. [168]. b) Photoluminescent preforms prepared via polymerization, where the luminescent dye was added to the monomer prior to the polymerization. The photograph is taken under illumination with UV light. Reproduced with permission from Ref. [81].

- Preparation of a preform.
- Drawing the preform into a fiber.

The preform can be manufactured in a variety of ways, including additive or subtractive manufacturing, molding, polymerization or extrusion. The cross-sectional shape of the preform is preserved during fiber drawing, enabling for example hollow-core, microstructured or triangular fibers. To add photoluminescent properties, the host polymer can be doped with a luminophore during preform preparation as required (Fig. 10**b**). The preform is fixed in the drawing machine by a clamping system and heated up above the host material's glass transition temperature, thus lowering its viscosity. The tapered bottom side of the preform is then pulled down and stretched by a set of godets revolving at predefined speeds, thus adjusting the ultimate diameter of the resulting fiber. The quenched fiber is finally wound on a bobbin. To sustain the thermal drawing process, the preform is continuously fed into the oven.

Over the years, the drawing process has been optimized towards preserving fine features implemented in the preform, like for example small cavities, which can generate microstructured fibers. The possibility to combine different materials in a preform, and thus in the resulting fiber, opens up a multitude of novel applications, e.g. by combining optical, electrical, or magnetic properties within a single fiber [176–182].

### 6.3. *Wet-spinning*

Wet-spinning is the oldest man-made fiber process; the first report dates back to 1883, where filaments have been produced for light bulbs [183]. In this process, which already became commercial in 1897 for rayon yarn production, a polymer solution is drawn from a spinneret into a "wet" coagulation bath, where it precipitates and solidifies [184]. More recently, fibers with enhanced electrical conductivity and humidity sensing capabilities have been wet-spun [185–187]. To produce PL-POFs, the polymer host, mixed with the luminophores, is dissolved at mild temperatures, before it is spun into the coagulation bath and drawn to a fiber (Fig. 11).

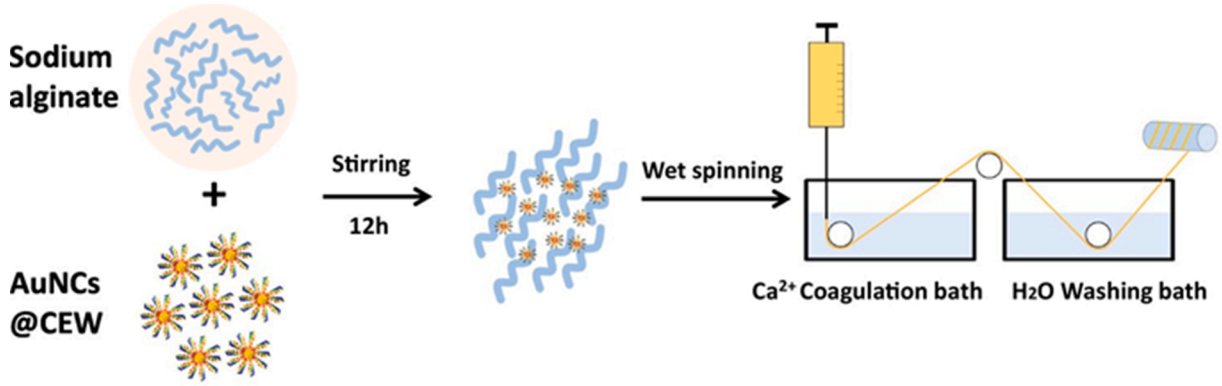


**Fig. 11.** Schematic representation of a PL-POF wet-spinning process. A solution containing a polymeric host material and a fluorescent dopant is stirred to assure uniform distribution, before it is injected into a coagulation bath, where the fiber solidifies. Subsequently, it is transferred to a washing bath and finally collected on a bobbin. Reproduced with permission from Ref. [144].

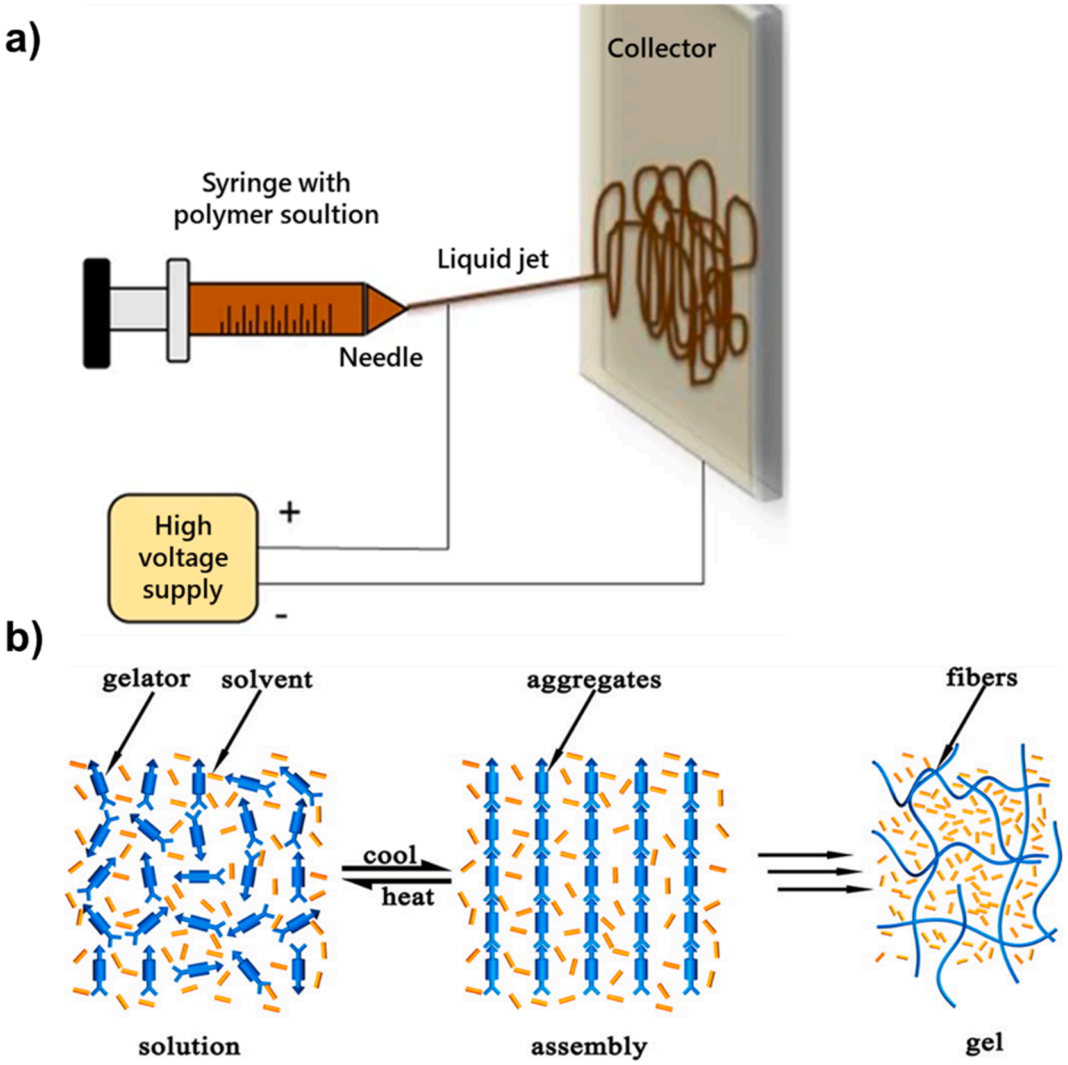


**Fig. 12.** a) Schematic illustration of an electrospinning setup utilized to produce fluorescent fiber membranes. Reproduced with permission from Ref. [150]. b) Schematic representation of a gelation process applied to obtain fibrous membranes with inherent electronic properties such as luminescence. Reproduced with permission from Ref. [193].

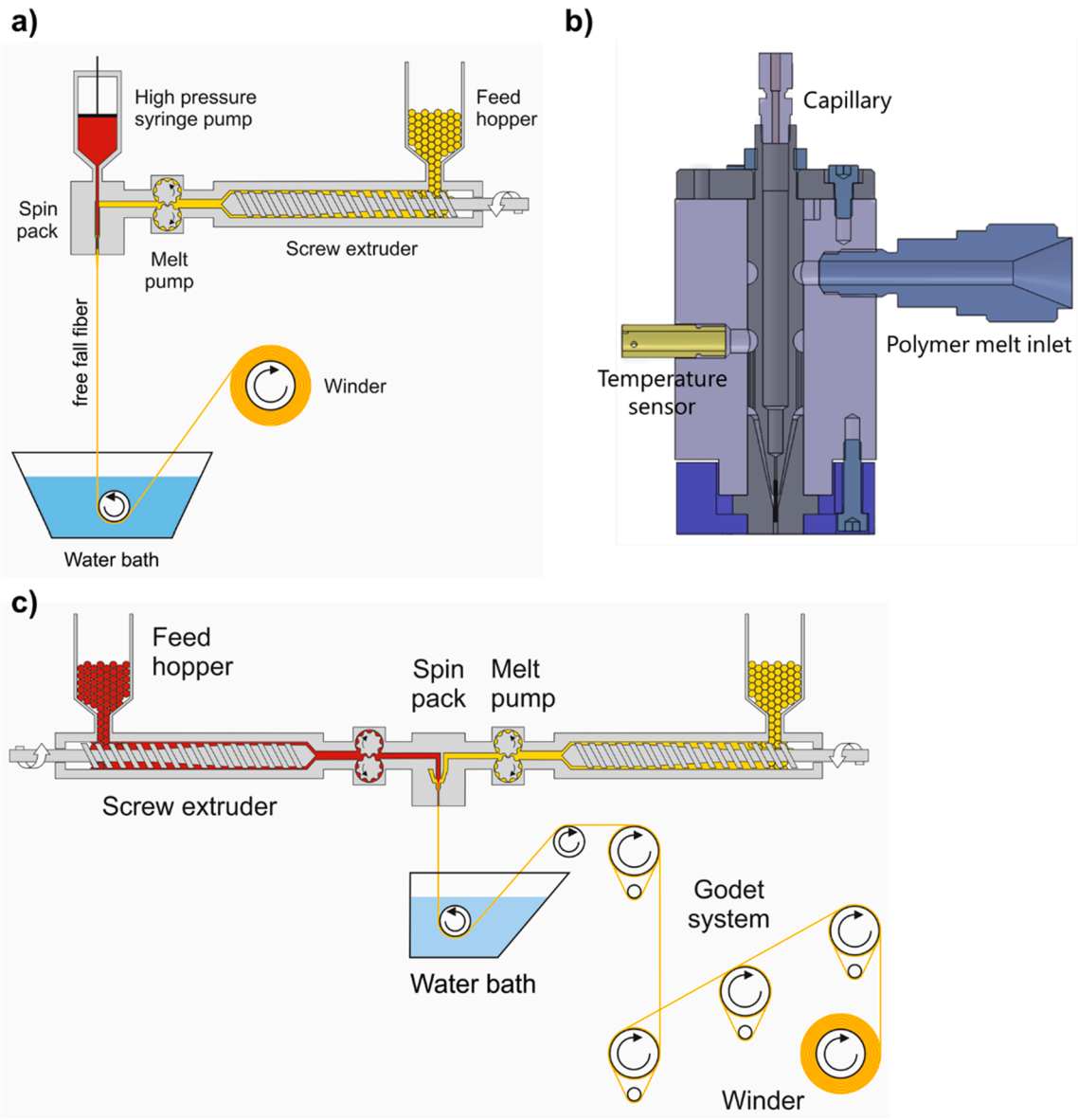


**Fig. 13.** a) Co-extrusion setup designed to produce flexible, liquid-core PL-POFs. The sheath (cladding) material is fed into the hopper, molten and pressurized by an extruder, and pumped into a spin pack b), where it engulfs the core liquid provided by a high-pressure pump. The two components coaxially exit the pack into a water bath for quenching and are subsequently wound onto a bobbin. By way of illustration, the polymer is represented in yellow, and the dye-doped liquid in red. Reproduced with permission from Ref. [58]. c) Melt-spinning setup designed to produce bicomponent, solid-core PL-POFs. Two granulated polymers (for the core and the cladding) are fed into the hoppers, melted and pressurized by extruders, and pumped into a spin pack. The fiber then exits the pack into a water bath for quenching, is subsequently drawn on a system of godets, and ultimately wound. By way of illustration, virgin and dye-doped polymer are represented in yellow and red, respectively. Reproduced with permission from Ref. [41]. (For interpretation of the references to color in this figure legend, the reader is referred to the web version of this article.)

### 6.4. *Electrospinning and gelation*

Electrospinning and gelation are both methods that are applied for the production of nanofiber membranes. Noteworthy, these PL fibers are distinct from typical PL-POFs, since they do not possess waveguiding properties. Nevertheless, they are mentioned in this review as an interesting approach to polymer-based PL fibers.

Electrospinning uses forces in a high voltage electrical field to draw liquid jets consisting of polymer solution, sol, suspension, or melt. The resulting fibers are drawn to nanometer diameters due to electrostatic forces acting on solvated ionic species; solidification occurs via rapid evaporation of the solvent [188,189]. The typical setup for electrospinning consists of two key parts, namely a conductive, electrically grounded spinneret, and a collector connected to the opposite pole (Fig. 12**a**). The spinneret is fed from a fluid pump that controls the jet flow-rate, and the electrospun fibers accumulate on the conducting collector, which is connected to high voltage [190]. The process is controlled by inherent instabilities and a delicate balance between solution extruding rate, solvated charge carriers, surface tension and solvent evaporation rate, which all affect the resulting fiber morphologies [191].

Gelation is another established technique used to prepare a three-dimensional porous network composed of long nanofibers. Interestingly, low molecular weight gelators, i.e. substances capable of forming a gel, can be structured in a self-assembly process. As an example, a gelator solution is first homogenized at elevated temperature, and when

subsequently cooled down, a nanofiber structure develops via supersaturation-mediated nucleation and growth (Fig. 12**b**) [192,193]. Gelation has attracted attention as a relatively easy way to prepare smart materials, which are responsive to a variety of stimuli in laboratory conditions [194–196]. Photoluminescent dyes can readily be introduced at different stages of the process.

### 6.5. Co-extrusion and melt-spinning

Melt-spinning is one of the most widely used techniques for synthetic fiber production [197]. Among these, bicomponent melt-spinning offers the possibility to co-extrude core and sheath of core-cladding POFs simultaneously, with the two polymers being fed from two separate extruders [8,109,198]. The viscous melts are optionally mixed with a dye and homogenized in the extrusion line, and subsequently pumped through a die, which defines the cross-sectional geometry of the fiber. The as-spun fiber finally solidifies, either in free fall through a quenching chamber flooded with cold air, or in a water bath, before it is drawn and wound onto a bobbin. Co-extrusion provides a scalable way to prepare graded-index or micro-structured fibers [199–202], but the costly and complicated equipment limits its applicability.

Based on the same bicomponent principle, flexible polymer fibers with luminescent liquid core were prepared, replacing the core material with dye-doped glycerol [58]. To enable the continuous production of liquid-filled polymeric fibers, spin pack and die were custom-designed [203,204]. The liquid was delivered at high pressure via a central capillary that was coaxially engulfed in the continuous flow of polymer melt. Finally, the resulting fibers were quenched in a water bath, and taken up at typical production rates of 30 m/min.

Bicomponent melt-spinning has great potential for future POF preparation, allowing production of mono-component graded-index, as well as co-extruded core-cladding fibers [8,9,198,205–211]. The use of photoluminescent dyes is however restricted by processing conditions and additional physical constraints like dye solubility in the melt [41]. Fig. 13 shows schematics of both co-extrusion of liquid-core fibers and bicomponent melt-spinning.

## 7. Conclusions

This review attempts to give an insight into a promising field that has been around for several decades but has not yet reached the homogeneity and awareness of an established research area. The possibility to combine photoluminescent properties with a fiber geometry can add totally new functionality to polymer optical fibers, a fact that is promising and has recently attracted the attention of various groups. We found that photoluminescent polymer optical fibers already offer a wide range of potential applications, ranging from light harvesters, through sensors, to lasers. Moreover, new emerging fields, such as luminescent receivers for short range optical communication signals are expected to further drive advances in the field.

By carefully selecting materials (host polymers and luminescent dyes), it is possible to tailor the mechanical and optical properties of the resulting fiber according to the intended use. It is expected that particularly new developments of fine-tuned QD dyes will further fertilize the field of PL-POFs in near future. QD qualities of interest include a short lifetime of the excited state (fast data communication), tunable absorption and emission (sensing), and stability (LSCs).

Techniques already established for commercial fiber production, like co-extrusion, melt-spinning or thermal drawing, were demonstrated to work for the production of specialized PL-POFs, when factors like temperature stability and material compatibility are considered.

From a technical standpoint, PL-POFs are ready to find more widespread market acceptance in areas like luminescent solar concentrators or integrated wearable textile sensing.

## CRediT authorship contribution statement

**Konrad Jakubowski:** Conceptualization, Investigation, Formal analysis, Writing - original draft. **Chieh-Szu Huang:** Investigation, Validation. **Luciano F. Boesel:** Conceptualization, Validation, Writing - review & editing, Supervision, Supervision. **Rudolf Hufenus:** Conceptualization, Validation, Writing - review & editing, Supervision. **Manfred Heuberger:** Conceptualization, Validation, Writing - review & editing, Supervision.

## Declaration of Competing Interest

The authors declare that they have no known competing financial interests or personal relationships that could have appeared to influence the work reported in this paper.

## Acknowledgements

The authors thank Professor Rene Rossi for insightful discussions.

## References

[1] K.C. Kao, G.A. Hockham, Dielectric-fibre surface waveguides for optical frequencies, Proc. Inst. Electr. Eng. 113 (1966) 1151–1158, https://doi.org/10.1049/piee.1966.0189.
[2] S. Abrate, Plastic optical fibers for data communications, in: Handb. Fiber Opt. Data Commun., Elsevier, 2013, pp. 37–54, https://doi.org/10.1016/B978-0-12-401673-6.00003-9.
[3] J.M. Toomasian, R.J. Schreiner, D.E. Meyer, M.E. Schmidt, S.E. Hagan, G. W. Griffith, R.H. Bartlett, K.E. Cook, A Polymethylpentene Fiber Gas Exchanger for Long-Term Extracorporeal Life Support, ASAIO J. 51 (2005) 390–397, https://doi.org/10.1097/01.mat.0000169111.66328.a8.
[4] M. van Eijkelenborg, M. Large, A. Argyros, J. Zagari, S. Manos, N. Issa, I. Bassett, S. Fleming, R. McPhedran, C.M. de Sterke, N.A. Nicorovici, Microstructured polymer optical fibre, Opt. Express 9 (2001) 319, https://doi.org/10.1364/OE.9.000319.
[5] G.T. Reynolds, P.E. Condon, Filament Scintillation Counter, Rev. Sci. Instrum. 28 (1957) 1098–1099, https://doi.org/10.1063/1.1715822.
[6] Y. Koike, Fundamentals of Plastic Optical Fibers, Wiley-VCH, First, 2015.
[7] D. Zaremba, R. Evert, Materials, chemical properties and analysis, in: Polym. Opt. Fibres, Elsevier, 2017, pp. 153–186, https://doi.org/10.1016/B978-0-08-100039-7.00005-1.
[8] F.A. Reifler, R. Hufenus, M. Krehel, E. Zgraggen, R.M. Rossi, L.J. Scherer, Polymer optical fibers for textile applications - Bicomponent melt spinning from cyclic olefin polymer and structural characteristics revealed by wide angle X-ray diffraction, Polym. (United Kingdom) 55 (2014) 5695–5707, https://doi.org/10.1016/j.polymer.2014.08.071.
[9] B.M. Quandt, F. Braun, D. Ferrario, R.M. Rossi, A. Scheel-Sailer, M. Wolf, G.-L. Bona, R. Hufenus, L.J. Scherer, L.F. Boesel, Body-monitoring with photonic textiles: a reflective heartbeat sensor based on polymer optical fibres, J. R. Soc. Interface 14 (2017), https://doi.org/10.1098/rsif.2017.0060.
[10] Y. Hanada, T. Ogawa, K. Koike, K. Sugioka, Making the invisible visible: a microfluidic chip using a low refractive index polymer, Lab Chip 16 (2016) 2481–2486, https://doi.org/10.1039/C6LC00481D.
[11] J. Hernández-Cor dero, Liquid-Core Optical Fibers, in: Spec. Opt. Fibers Handb., Elsevier, 2007, pp. 599–616, https://doi.org/10.1016/B978-012369406-5/50021-7.
[12] H. Fitz, Light conductor with liquid core and a fluorine placement, DE3617005A1, 1986. https://patents.google.com/patent/DE3617005A1/en.
[13] J. Stone, Optical transmission loss in liquid-core hollow fibers, IEEE J. Quantum Electron. 8 (1972) 386–388, https://doi.org/10.1109/JQE.1972.1076966.
[14] G.E. Walrafen, J. Stone, Intensification of Spontaneous Raman Spectra by Use of Liquid Core Optical Fibers, Appl. Spectrosc. 26 (1972) 585–589, https://doi.org/10.1366/000370272774351688.
[15] E.P. Ippen, Low-power quasi-cw Raman oscillator, Appl. Phys. Lett. 16 (1970) 303–305, https://doi.org/10.1063/1.1653204.
[16] F.M. Cox, A. Argyros, M.C.J. Large, Liquid-filled hollow core microstructured polymer optical fiber, Opt. Express 14 (2006) 4135, https://doi.org/10.1364/OE.14.004135.
[17] I. Martincek, D. Pudis, M. Chalupova, Technology for the Preparation of PDMS Optical Fibers and Some Fiber Structures, IEEE Photonics Technol. Lett. 26 (2014) 1446–1449, https://doi.org/10.1109/LPT.2014.2326695.
[18] W. Ding, J. Sun, G. Chen, L. Zhou, J. Wang, X. Gu, J. Wan, X. Pu, B. Tang, Z. L. Wang, Stretchable multi-luminescent fibers with AIEgens, J. Mater. Chem. C 7 (2019) 10769–10776, https://doi.org/10.1039/C9TC03461G.
[19] B.M. Quandt, R. Hufenus, B. Weisse, F. Braun, M. Wolf, A. Scheel-Sailer, G.-L. Bona, R.M. Rossi, L.F. Boesel, Optimization of novel melt-extruded polymer optical fibers designed for pressure sensor applications, Eur. Polym. J. 88 (2017) 44–55, https://doi.org/10.1016/j.eurpolymj.2016.12.032.

[20] C. Meichner, A.E. Schedl, C. Neuber, K. Kreger, H.-W. Schmidt, L. Kador, Refractive-index determination of solids from first- and second-order critical diffraction angles of periodic surface patterns, AIP Adv. 5 (2015), 087135, https://doi.org/10.1063/1.4928654.

[21] C.A. Bunge, M. Beckers, B. Lustermann, Basic principles of optical fibres, Elsevier Ltd, 2016 https://doi.org/10.1016/B978-0-08-100039-7.00003-8.

[22] K.R. McIntosh, N. Yamada, B.S. Richards, Theoretical comparison of cylindrical and square-planar luminescent solar concentrators, Appl. Phys. B: Lasers Opt. 88 (2007) 285–290, https://doi.org/10.1007/s00340-007-2705-8.

[23] G. Griffini, Host Matrix Materials for Luminescent Solar Concentrators: Recent Achievements and Forthcoming Challenges, Front. Mater. 6 (2019), https://doi.org/10.3389/fmats.2019.00029.

[24] Y. Li, X. Zhang, Y. Zhang, R. Dong, C.K. Luscombe, Review on the Role of Polymers in Luminescent Solar Concentrators, J. Polym. Sci., Part A: Polym. Chem. 57 (2019) 201–215, https://doi.org/10.1002/pola.29192.

[25] J.R. Lakowicz, Introduction to Fluorescence, in: Princ. Fluoresc. Spectrosc., Springer US, Boston, MA, 2006, pp. 1–26, https://doi.org/10.1007/978-0-387-46312-4_1.

[26] D. Frackowiak, The Jablonski diagram, J. Photochem. Photobiol. B Biol. 2 (1988) 399, https://doi.org/10.1016/1011-1344(88)85060-7.

[27] F. Clabau, X. Rocquefelte, S. Jobic, P. Deniard, M.-H. Whangbo, A. Garcia, T. Le Mercier, Mechanism of Phosphorescence Appropriate for the Long-Lasting Phosphors Eu 2+ -Doped SrAl 2 O 4 with Codopants Dy 3+ and B 3+, Chem. Mater. 17 (2005) 3904–3912, https://doi.org/10.1021/cm050763r.

[28] A. Juris, P. Ceroni, V. Balzani, Photochemistry and photophysics : concepts, research, applications, first ed., Wiley-VCH, 2014.

[29] W.Y. Liang, Excitons, Phys. Educ. 5 (1970) 003, https://doi.org/10.1088/0031-9120/5/4/003.

[30] R.S. Knox, Theory of excitons, in: Solid State Phys. Suppl., vol. 5, Academic Press, 1963, p. 207.

[31] J. Singh, Theory of Excitons, in: Excit. Energy Transf. Process. Condens. Matter, Springer US, Boston, MA, 1994, pp. 1–45, https://doi.org/10.1007/978-1-4899-0996-1_1.

[32] I. Vragović, R. Scholz, Frenkel exciton model of optical absorption and photoluminescence in α-PTCDA, Phys. Rev. B. 68 (2003), 155202, https://doi.org/10.1103/PhysRevB.68.155202.

[33] H.A. Jahn, E. Teller, Stability of polyatomic molecules in degenerate electronic states - I—Orbital degeneracy, Proc. R. Soc. London. Ser. A - Math. Phys. Sci. 161 (1937) 220–235, https://doi.org/10.1098/rspa.1937.0142.

[34] J. Feng, H. Zhang, Hybrid materials based on lanthanide organic complexes: a review, Chem. Soc. Rev. 42 (2013) 387–410, https://doi.org/10.1039/C2CS35069F.

[35] D. Bera, L. Qian, T.-K. Tseng, P.H. Holloway, Quantum Dots and Their Multimodal Applications: A Review, Materials (Basel). 3 (2010) 2260–2345, https://doi.org/10.3390/ma3042260.

[36] J.R. Lakowicz, Principles of Fluorescence Spectroscopy, Second,, Springer US, Boston, MA, 2006.

[37] J.W.E. Wiegman, E. Van Der Kolk, Building integrated thin film luminescent solar concentrators: Detailed efficiency characterization and light transport modelling, Sol. Energy Mater. Sol. Cells 103 (2012) 41–47, https://doi.org/10.1016/j.solmat.2012.04.016.

[38] P. Moraitis, R.E.I. Schropp, W.G.J.H.M. van Sark, Nanoparticles for Luminescent Solar Concentrators - A review, Opt. Mater. (Amst). 84 (2018) 636–645, https://doi.org/10.1016/j.optmat.2018.07.034.

[39] M. Rafiee, S. Chandra, H. Ahmed, S.J. McCormack, An overview of various configurations of Luminescent Solar Concentrators for photovoltaic applications, Opt. Mater. (Amst) 91 (2019) 212–227, https://doi.org/10.1016/j.optmat.2019.01.007.

[40] C.-S. Huang, K. Jakubowski, S. Ulrich, S. Yakunin, M. Clerc, C. Toncelli, R. M. Rossi, M.V. Kovalenko, L.F. Boesel, Nano-domains assisted energy transfer in amphiphilic polymer conetworks for wearable luminescent solar concentrators, Nano Energy (2020), 105039, https://doi.org/10.1016/j.nanoen.2020.105039.

[41] K. Jakubowski, C.-S. Huang, A. Gooneie, L.F. Boesel, M. Heuberger, R. Hufenus, Luminescent solar concentrators based on melt-spun polymer optical fibers, Mater. Des. (2020), 108518, https://doi.org/10.1016/j.matdes.2020.108518.

[42] R.F. Chen, J.R. Knutson, Mechanism of fluorescence concentration quenching of carboxyfluorescein in liposomes: Energy transfer to nonfluorescent dimers, Anal. Biochem. 172 (1988) 61–77, https://doi.org/10.1016/0003-2697(88)90412-5.

[43] K. Muto, Electric-discharge sensor utilizing fluorescent optical fiber, J. Light. Technol. 7 (1989) 1029–1032, https://doi.org/10.1109/50.29629.

[44] R. Reisfeld, New developments in luminescence for solar energy utilization, Opt. Mater. (Amst) 32 (2010) 850–856, https://doi.org/10.1016/j.optmat.2010.04.034.

[45] E.-H. Banaei, A.F. Abouraddy, Design of a polymer optical fiber luminescent solar concentrator, Prog. Photovolt Res. Appl. 23 (2015) 403–416, https://doi.org/10.1002/pip.2435.

[46] C. Yang, R.R. Lunt, Limits of Visibly Transparent Luminescent Solar Concentrators, Adv. Opt. Mater. 5 (2017) 1–10, https://doi.org/10.1002/adom.201600851.

[47] T.G. Mayerhöfer, J. Popp, Beer's Law - Why Absorbance Depends (Almost) Linearly on Concentration, ChemPhysChem 20 (2019) 511–515, https://doi.org/10.1002/cphc.201801073.

[48] X. Wang, R.R. Valiev, T.Y. Ohulchanskyy, H. Ågren, C. Yang, G. Chen, Dye-sensitized lanthanide-doped upconversion nanoparticles, Chem. Soc. Rev. 46 (2017) 4150–4167, https://doi.org/10.1039/c7cs00053g.

[49] F.J. Caixeta, A.R.N. Bastos, A.M.P. Botas, L.S. Rosa, V.S. Souza, F.H. Borges, A.N. C. Neto, A. Ferrier, P. Goldner, L.D. Carlos, R.R. Gonçalves, R.A.S. Ferreira, High-Quantum-Yield Upconverting Er 3+ /Yb 3+ -Organic–Inorganic Hybrid Dual Coatings for Real-Time Temperature Sensing and Photothermal Conversion, J. Phys. Chem. C 124 (2020) 19892–19903, https://doi.org/10.1021/acs.jpcc.0c03874.

[50] I. Papakonstantinou, C. Tummeltshammer, Fundamental limits of concentration in luminescent solar concentrators revised: the effect of reabsorption and nonunity quantum yield, Optica 2 (2015) 841, https://doi.org/10.1364/OPTICA.2.000841.

[51] G. Aldabaldetreku, I. Bikandi, M.A. Illarramendi, G. Durana, J. Zubia, A comprehensive analysis of scattering in polymer optical fibers, Opt. Express 18 (2010) 24536, https://doi.org/10.1364/OE.18.024536.

[52] C.-a. Bunge, R. Kruglov, H. Poisel, Rayleigh and Mie scattering in polymer optical fibers, J. Light. Technol. 24 (2006) 3137–3146, https://doi.org/10.1109/JLT.2006.878077.

[53] J. Roncali, F. Garnier, Photon-transport properties of luminescent solar concentrators: analysis and optimization, Appl. Opt. 23 (1984) 2809, https://doi.org/10.1364/AO.23.002809.

[54] M.J. Currie, J.K. Mapel, T.D. Heidel, S. Goffri, M.A. Baldo, High-Efficiency Organic Solar Concentrators for Photovoltaics, Science (80-.) 321 (2008) 226–228, https://doi.org/10.1126/science.1158342.

[55] W. Wu, T. Wang, X. Wang, S. Wu, Y. Luo, X. Tian, Q. Zhang, Hybrid solar concentrator with zero self-absorption loss, Sol. Energy 84 (2010) 2140–2145, https://doi.org/10.1016/j.solener.2010.08.012.

[56] Z. Krumer, W.G.J.H.M. van Sark, R.E.I. Schropp, C. de Mello Donegá, Compensation of self-absorption losses in luminescent solar concentrators by increasing luminophore concentration, Sol. Energy Mater. Sol. Cells 167 (2017) 133–139, https://doi.org/10.1016/j.solmat.2017.04.010.

[57] K. Jakubowski, C.-S. Huang, A. Gooneie, L.F. Boesel, M. Heuberger, R. Hufenus, Luminescent solar concentrators based on melt-spun polymer optical fibers, Mater. Des. 189 (2020), https://doi.org/10.1016/j.matdes.2020.108518.

[58] K. Jakubowski, W. Kerkemeyer, E. Perret, M. Heuberger, R. Hufenus, Liquid-core polymer optical fibers for luminescent waveguide applications, Mater. Des. (2020), 109131, https://doi.org/10.1016/j.matdes.2020.109131.

[59] The National Renewable Energy Laboratory, Best Research-Cell Efficiency Chart, 2019. https://www.nrel.gov/pv/cell-efficiency.html (accessed July 1, 2019).

[60] P.G.V. Sampaio, M.O.A. Gonzalez, Photovoltaic solar energy: Conceptual framework, Renew. Sustain. Energy Rev. 74 (2017) 590–601, https://doi.org/10.1016/j.rser.2017.02.081.

[61] W.H. Weber, J. Lambe, Luminescent greenhouse collector for solar radiation, Appl. Opt. 15 (1976) 2299, https://doi.org/10.1364/AO.15.002299.

[62] A. Goetzberger, W. Greubel, Applied Physics Solar Energy Conversion with Fluorescent Collectors, Appl. Phys. 14 (1977) 123–139.

[63] R. Reisfeld, S. Neuman, Planar solar energy converter and concentrator based on uranyl-doped glass, Nature 274 (1978) 144–145, https://doi.org/10.1038/274144a0.

[64] R. Reisfeld, Y. Kalisky, Improved planar solar converter based on uranyl neodymium and holmium glasses, Nature 283 (1980) 281–282, https://doi.org/10.1038/283281a0.

[65] J. Roncali, Luminescent Solar Collectors: Quo Vadis? Adv. Energy Mater. 10 (2020) 2001907, https://doi.org/10.1002/aenm.202001907.

[66] M.R. Kulish, V.P. Kostylyov, A.V. Sachenko, I.O. Sokolovskyi, D.V. Khomenko, A. I. Shkrebtii, Luminescent converter of solar light into electrical energy, Review (2016) 229–247.

[67] N. Aste, M. Buzzetti, C. Del Pero, R. Fusco, F. Leonforte, D. Testa, Triggering a large scale luminescent solar concentrators market: The smart window project, J. Clean. Prod. 219 (2019) 35–45, https://doi.org/10.1016/j.jclepro.2019.02.089.

[68] R.A.S. Ferreira, S.F.H. Correia, A. Monguzzi, X. Liu, F. Meinardi, Spectral converters for photovoltaics – What's ahead, Mater. Today (2019), https://doi.org/10.1016/j.mattod.2019.10.002.

[69] S.F.H. Correia, P. Lima, E. Pecoraro, S. Ribeiro, P. André, R. Ferreira, L. Carlos, Scale up the collection area of luminescent solar concentrators towards metre-length flexible waveguiding photovoltaics, Prog. Photovolt. Res. Appl. 24 (2016) 1178–1193, https://doi.org/10.1002/pip.

[70] R. Reisfeld, D. Shamrakov, C. Jorgensen, Photostable solar concentrators based on fluorescent glass films, Sol. Energy Mater. Sol. Cells 33 (1994) 417–427, https://doi.org/10.1016/0927-0248(94)90002-7.

[71] S.F.H. Correia, A.R.N. Bastos, L. Fu, L.D. Carlos, P.S. Andre, R.A.S. Ferreira, Lanthanide-based downshifting layers tested in a solar car race, Opto-Electronic Adv. 2 (2019) 19000601–19000608, https://doi.org/10.29026/oea.2019.190006.

[72] W.T. Xie, Y.J. Dai, R.Z. Wang, K. Sumathy, Concentrated solar energy applications using Fresnel lenses: A review, Renew. Sustain. Energy Rev. 15 (2011) 2588–2606, https://doi.org/10.1016/j.rser.2011.03.031.

[73] D.K. Patel, P.K. Brahmbhatt, H. Panchal, A review on compound parabolic solar concentrator for sustainable development, Int. J. Ambient Energy 0750 (2017) 1–14, https://doi.org/10.1080/01430750.2017.1318786.

[74] Y. Shen, Y. Jia, X. Sheng, L. Shen, J.A. Rogers, N.C. Giebink, Nonimaging Optical Gain in Luminescent Concentration through Photonic Control of Emission Étendue, ACS Photonics 1 (2014) 746–753, https://doi.org/10.1021/ph500196r.

[75] P.P. Manousiadis, S. Rajbhandari, R. Mulyawan, D.A. Vithanage, H. Chun, G. Faulkner, D.C. O'Brien, G.A. Turnbull, S. Collins, I.D.W. Samuel, Wide field-of-view fluorescent antenna for visible light communications beyond the étendue limit, Optica. 3 (2016) 702, https://doi.org/10.1364/OPTICA.3.000702.

[76] Y. Dong, M. Shi, X. Yang, P. Zeng, J. Gong, S. Zheng, M. Zhang, R. Liang, Q. Ou, N. Chi, S. Zhang, Nanopatterned luminescent concentrators for visible light communications, Opt. Express 25 (2017) 21926, https://doi.org/10.1364/OE.25.021926.
[77] G. Smestad, H. Ries, R. Winston, E. Yablonovitch, The thermodynamic limits of light concentrators, Sol. Energy Mater. 21 (1990) 99–111, https://doi.org/10.1016/0165-1633(90)90047-5.
[78] R.H. Inman, G.V. Shcherbatyuk, D. Medvedko, A. Gopinathan, S. Ghosh, Cylindrical luminescent solar concentrators with near-infrared quantum dots, Opt. Express 19 (2011) 24308, https://doi.org/10.1364/OE.19.024308.
[79] E.-H. Banaei, A.F. Abouraddy, Fiber luminescent solar concentrator with 5.7% conversion efficiency, High Low Conc. Syst. Sol. Electr. Appl. VIII. VIII (2013) 1952–1955, https://doi.org/10.1117/12.2022601.
[80] O.Y. Edelenbosch, M. Fisher, L. Patrignani, W.G.J.H.M. van Sark, A.J. Chatten, Luminescent solar concentrators with fiber geometry, Opt. Express 21 (2013) A503, https://doi.org/10.1364/OE.21.00A503.
[81] I. Parola, D. Zaremba, R. Evert, J. Kielhorn, F. Jakobs, M.A. Illarramendi, J. Zubia, W. Kowalsky, H.H. Johannes, High performance fluorescent fiber solar concentrators employing double-doped polymer optical fibers, Sol. Energy Mater. Sol. Cells 178 (2018) 20–28, https://doi.org/10.1016/j.solmat.2018.01.013.
[82] I. Parola, E. Arrospide, F. Recart, M. Illarramendi, G. Durana, N. Guarrotxena, O. García, J. Zubia, Fabrication and Characterization of Polymer Optical Fibers Doped with Perylene-Derivatives for Fluorescent Lighting Applications, Fibers. 5 (2017) 28, https://doi.org/10.3390/fib5030028.
[83] I. Parola, M.A. Illarramendi, J. Zubia, E. Arrospide, G. Durana, N. Guarrotxena, O. García, R. Evert, D. Zaremba, H.-H. Johannes, F. Recart, Polymer optical fibers doped with organic materials as luminescent solar concentrators, Proc. SPIE Int. Soc. Opt. Eng. 10101 (2017) 101010Z, https://doi.org/10.1117/12.2252956.
[84] I. Parola, M.A. Illarramendi, F. Jakobs, J. Kielhorn, D. Zaremba, H.-H. Johannes, J. Zubia, Characterization of Double-Doped Polymer Optical Fibers as Luminescent Solar Concentrators, Polymers (Basel) 11 (2019) 1187, https://doi.org/10.3390/polym11071187.
[85] S.F.H. Correia, A.R. Frias, L. Fu, R. Rondão, E. Pecoraro, S.J.L. Ribeiro, P. S. André, R.A.S. Ferreira, L.D. Carlos, Large-Area Tunable Visible-to-Near-Infrared Luminescent Solar Concentrators, Adv. Sustain. Syst. 1800002 (2018), https://doi.org/10.1002/adsu.201800002, 1800002 (1–9).
[86] J. Videira, E. Bilotti, A. Chatten, Cylindrical array luminescent solar concentrators: performance boosts by geometric effects, Opt. Express 24 (2016) 285–290, https://doi.org/10.1364/OE.24.0A1188.
[87] R. Galatus, D. Petreus, D. Moga, T. Marita, N. Stroia, Extending Battery Life Time in the Wireless Sensor Applications with Fluorescent Optical Fiber Concentrator, in: 2018 IEEE Int. Instrum. Meas. Technol. Conf., 2018, pp. 1–6.
[88] O. Besida, Y. Piret, F. Rondeaux, Fluorescent photonic crystal fibers trapping light in a luminescent solar concentrator, AIP Conf. Proc. 2149 (2019), 050004, https://doi.org/10.1063/1.5124189.
[89] H. Poisel, K.F. Klein, V.M. Levin, Fluorescent Optical Fibers for Data Transmission, 2001, pp. 211–219. https://doi.org/10.1021/bk-2001-0795.ch015.
[90] T. Peyronel, K.J. Quirk, S.C. Wang, T.G. Tiecke, Luminescent detector for free-space optical communication, Optica 3 (2016) 787, https://doi.org/10.1364/OPTICA.3.000787.
[91] A. Riaz, G. Faulkner, S. Collins, A Fluorescent Antenna for White Light Visible Light Communications, in: 2019 Glob. LIFI Congr., IEEE, 2019, pp. 1–4, https://doi.org/10.1109/GLC.2019.8864125.
[92] A. Riaz, G. Faulkner, D. O'Brien, S. Collins, The relationships between the amplitude of receiver output voltage and the maximum achievable OOK data rate, in: H. Hemmati, D.M. Boroson (Eds.), Free. Laser Commun. XXXII, SPIE, 2020, pp. 43. https://doi.org/10.1117/12.2545604.
[93] M. Portnoi, P.A. Haigh, T.J. Macdonald, F. Ambroz, I.P. Parkin, I. Darwazeh, I. Papakonstantinou, Bandwidth limits of luminescent solar concentrators as detectors in free-space optical communication systems, Light Sci. Appl. 10 (2021) 3, https://doi.org/10.1038/s41377-020-00444-y.
[94] UniQD, (n.d.). https://ubiqd.com/ (accessed April 30, 2020).
[95] Eni, (n.d.). https://www.eni.com/en-IT/operations/concentrators-solar-luminescent.html (accessed April 30, 2020).
[96] signify, (n.d.). https://www.signify.com/global/our-company/intellectual-property/licensing/luminescent-solar-concentrator (accessed April 30, 2020).
[97] I. Papakonstantinou, M. Portnoi, M.G. Debije, The Hidden Potential of Luminescent Solar Concentrators, Adv. Energy Mater. 11 (2021) 2002883, https://doi.org/10.1002/aenm.202002883.
[98] R. Kinderman, L.H. Slooff, A.R. Burgers, N.J. Bakker, A. Büchtemann, R. Danz, J. A.M. van Roosmalen, I-V Performance and Stability Study of Dyes for Luminescent Plate Concentrators, J. Sol. Energy Eng. 129 (2007) 277–282, https://doi.org/10.1115/1.2737469.
[99] A.A. Earp, T. Rawling, J.B. Franklin, G.B. Smith, Perylene dye photodegradation due to ketones and singlet oxygen, Dye. Pigment. 84 (2010) 59–61, https://doi.org/10.1016/j.dyepig.2009.06.012.
[100] J.-M. Delgado-Sanchez, Luminescent solar concentrators: Photo-stability analysis and long-term perspectives, Sol. Energy Mater. Sol. Cells 202 (2019), 110134, https://doi.org/10.1016/j.solmat.2019.110134.
[101] L.H. Slooff, N.J. Bakker, P.M. Sommeling, A. Büchtemann, A. Wedel, W.G.J.H. M. van Sark, Long-term optical stability of fluorescent solar concentrator plates, Phys. Status Solidi 211 (2014) 1150–1154, https://doi.org/10.1002/pssa.201330447.
[102] G. Liu, H. Zhao, F. Diao, Z. Ling, Y. Wang, Stable tandem luminescent solar concentrators based on CdSe/CdS quantum dots and carbon dots, J. Mater. Chem. C 6 (2018) 10059–10066, https://doi.org/10.1039/C8TC02532K.
[103] S. Sadeghi, H. Bahmani Jalali, R. Melikov, B. Ganesh Kumar, M. Mohammadi Aria, C.W. Ow-Yang, S. Nizamoglu, Stokes-Shift-Engineered Indium Phosphide Quantum Dots for Efficient Luminescent Solar Concentrators, ACS Appl. Mater. Interfaces 10 (2018) 12975–12982, https://doi.org/10.1021/acsami.7b19144.
[104] Z. Krumer, S.J. Pera, R.J.A. van Dijk-Moes, Y. Zhao, A.F.P. de Brouwer, E. Groeneveld, W.G.J.H.M. van Sark, R.E.I. Schropp, C. de Mello Donegá, Tackling self-absorption in luminescent solar concentrators with type-II colloidal quantum dots, Sol. Energy Mater. Sol. Cells 111 (2013) 57–65, https://doi.org/10.1016/j.solmat.2012.12.028.
[105] F. Meinardi, A. Colombo, K.A. Velizhanin, R. Simonutti, M. Lorenzon, L. Beverina, R. Viswanatha, V.I. Klimov, S. Brovelli, Large-area luminescent solar concentrators based on Stokes-shift-engineered nanocrystals in a mass-polymerized PMMA matrix, Nat. Photonics 8 (2014) 392–399, https://doi.org/10.1038/nphoton.2014.54.
[106] F. Meinardi, Q.A. Akkerman, F. Bruni, S. Park, M. Mauri, Z. Dang, L. Manna, S. Brovelli, Doped Halide Perovskite Nanocrystals for Reabsorption-Free Luminescent Solar Concentrators, ACS Energy Lett. 2 (2017) 2368–2377, https://doi.org/10.1021/acsenergylett.7b00701.
[107] F. Purcell-Milton, Y.K. Gun'ko, Quantum dots for Luminescent Solar Concentrators, J. Mater. Chem. 22 (2012) 16687, https://doi.org/10.1039/c2jm32366d.
[108] Y. You, X. Tong, W. Wang, J. Sun, P. Yu, H. Ji, X. Niu, Z.M. Wang, Eco-Friendly Colloidal Quantum Dot-Based Luminescent Solar Concentrators, Adv. Sci. 6 (2019) 1801967, https://doi.org/10.1002/advs.201801967.
[109] B.M. Quandt, L.J. Scherer, L.F. Boesel, M. Wolf, G.-L. Bona, R.M. Rossi, Body-Monitoring and Health Supervision by Means of Optical Fiber-Based Sensing Systems in Medical Textiles, Adv. Healthc. Mater. 4 (2015) 330–355, https://doi.org/10.1002/adhm.201400463.
[110] K.S.C. Kuang, S.T. Quek, C.G. Koh, W.J. Cantwell, P.J. Scully, Plastic Optical Fibre Sensors for Structural Health Monitoring: A Review of Recent Progress, J. Sensors. 2009 (2009) 1–13, https://doi.org/10.1155/2009/312053.
[111] M.M. Werneck, R.C. da S.B. Allil (Eds.), Plastic Optical Fiber Sensors, CRC Press, 2019. https://doi.org/10.1201/b22357.
[112] K.T.V. Grattan, B.T. Meggitt (Eds.), Optical Fiber Sensor Technology, Springer US, Boston, MA, 1999, https://doi.org/10.1007/978-1-4757-6077-4.
[113] S.H. Law, S.C. Fleming, N. Suchowerska, D.R. McKenzie, Optical fiber design and the trapping of Cerenkov radiation, Appl. Opt. 45 (2006) 9151, https://doi.org/10.1364/AO.45.009151.
[114] Radiation-Induced Attenuation of Perfluorinated Polymer Optical Fibers for Radiation Monitoring, Sensors. 17 (2017) 1959. https://doi.org/10.3390/s17091959.
[115] H. Leutz, Scintillating fibres Nucl Instruments Methods Phys, Res. Sect. A Accel. Spectrometers, Detect. Assoc. Equip. 364 (1995) 422–448, https://doi.org/10.1016/0168-9002(95)00383-5.
[116] M. Ellis, P.R. Hobson, P. Kyberd, J.J. Nebrensky, A. Bross, J. Fagan, T. Fitzpatrick, R. Flores, R. Kubinski, J. Krider, R. Rucinski, P. Rubinov, C. Tolian, T.L. Hart, D. M. Kaplan, W. Luebke, B. Freemire, M. Wojcik, G. Barber, D. Clark, I. Clark, P. J. Dornan, A. Fish, S. Greenwood, R. Hare, A. Jamdagni, V. Kasey, M. Khaleeq, J. Leaver, K.R. Long, E. McKigney, T. Matsushita, C. Rogers, T. Sashalmi, P. Savage, M. Takahashi, A. Tapper, K. Yoshimura, P. Cooke, R. Gamet, H. Sakamoto, Y. Kuno, A. Sato, T. Yano, M. Yoshida, C. MacWaters, L. Coney, G. Hanson, A. Klier, D. Cline, X. Yang, D. Adey, The design, construction and performance of the MICE scintillating fibre trackers, Nucl. Instruments Methods Phys. Res. Sect. A Accel. Spectrometers, Detect. Assoc. Equip. 659 (2011) 136–153, https://doi.org/10.1016/j.nima.2011.04.041.
[117] E. Overton, Progress with the MICE scintillating fiber trackers, Nucl. Instruments Methods Phys. Res. Sect. A Accel. Spectrometers, Detect. Assoc. Equip. 732 (2013) 412–414, https://doi.org/10.1016/j.nima.2013.05.112.
[118] C. Joram, G. Haefeli, B. Leverington, Scintillating Fibre Tracking at High Luminosity Colliders, J. Instrum. 10 (2015) C08005, https://doi.org/10.1088/1748-0221/10/08/C08005.
[119] A. Papa, F. Barchetti, F. Gray, E. Ripiccini, G. Rutar, A multi-purposed detector with silicon photomultiplier readout of scintillating fibers, Nucl. Instruments Methods Phys. Res. Sect. A Accel. Spectrometers, Detect. Assoc. Equip. 787 (2015) 130–133, https://doi.org/10.1016/j.nima.2014.11.074.
[120] E.O. Cohen, E. Piasetzky, Y. Shamai, N. Pilip, Development of a scintillating-fiber beam detector for the MUSE experiment, Nucl. Instruments Methods Phys. Res. Sect. A Accel. Spectrometers, Detect. Assoc. Equip. 815 (2016) 75–82, https://doi.org/10.1016/j.nima.2016.01.044.
[121] R. McNabb, J. Blackburn, J.D. Crnkovic, D.W. Hertzog, B. Kiburg, J. Kunkle, E. Thorsland, D.M. Webber, K.R. Lynch, A tungsten/scintillating fiber electromagnetic calorimeter prototype for a high-rate muon experiment, Nucl. Instruments Methods Phys. Res. Sect. A Accel. Spectrometers, Detect. Assoc. Equip. 602 (2009) 396–402, https://doi.org/10.1016/j.nima.2009.01.007.
[122] K. Yu, Scintillation Detectors in Modern High Energy Physics Experiments and Prospect of Their use in Future Experiments, J. Lasers, Opt. Photonics. 04 (2017), https://doi.org/10.4172/2469-410X.1000148.
[123] K. Tanderup, S. Beddar, C.E. Andersen, G. Kertzscher, J.E. Cygler, In vivo dosimetry in brachytherapy, Med. Phys. 40 (2013), 070902, https://doi.org/10.1118/1.4810943.
[124] S. O'Keeffe, D. McCarthy, P. Woulfe, M.W.D. Grattan, A.R. Hounsell, D. Sporea, L. Mihai, I. Vata, G. Leen, E. Lewis, A review of recent advances in optical fibre

sensors for in vivo dosimetry during radiotherapy, Br. J. Radiol. 88 (2015) 20140702, https://doi.org/10.1259/bjr.20140702.
[125] M.F. Laguesse, M.J. Bourdinaud, Characterization of fluorescent plastic optical fibers for x-ray beam detection, in: M. Kitazawa, J.F. Kreidl, R.E. Steele (Eds.), 1991: pp. 96–107. https://doi.org/10.1117/12.50997.
[126] E. Yousif, R. Haddad, Photodegradation and photostabilization of polymers, especially polystyrene: review, Springerplus 2 (2013) 398, https://doi.org/10.1186/2193-1801-2-398.
[127] Y.-H. Chiu, T.-F.M. Chang, C.-Y. Chen, M. Sone, Y.-J. Hsu, Mechanistic Insights into Photodegradation of Organic Dyes Using Heterostructure Photocatalysts, Catalysts 9 (2019) 430, https://doi.org/10.3390/catal9050430.
[128] P. Stajanca, POF and Radiation Sensing, in: M.M. Werneck, R.C. da S.B. Allil (Eds.), Plast. Opt. Fiber Sensors, CRC Press, 2019, pp. 285–313.
[129] C. Fitzpatrick, C.O. Donoghue, E. Lewis, A novel multi-point ultraviolet optical fibre sensor based on cladding luminescence, Meas. Sci. Technol. 14 (2003) 1477–1483, https://doi.org/10.1088/0957-0233/14/8/337.
[130] P. Miluski, D. Dorosz, M. Kochanowicz, J. Zmojda, J. Dorosz, Luminescent optical fibre sensor for UV-A detection, in: R.S. Romaniuk (Ed.), 2014: p. 92900G. https://doi.org/10.1117/12.2075077.
[131] P. Miluski, M. Kochanowicz, J. Żmojda, D. Dorosz, UV Radiation Detection Using Optical Sensor Based on Eu3+ Doped PMMA, Metrol. Meas. Syst. 23 (2016) 615–621, https://doi.org/10.1515/mms-2016-0049.
[132] L. Szolga, R. Galatus, G. Oltean, Fluorescent optical fiber sensor for arcing and flame monitoring in electrical distribution boards, in: 2018 IEEE Int. Instrum. Meas. Technol. Conf., IEEE, 2018, pp. 1–5, https://doi.org/10.1109/I2MTC.2018.8409836.
[133] G.D.P. Mahidhar, R. Sarathi, B. Srinivasan, Fluorescence Fiber Based Identification of Partial Discharges in Liquid Nitrogen for High-Temperature Superconducting Power Apparatus, IEEE Sensors Lett. 4 (2020) 1–4, https://doi.org/10.1109/LSENS.2020.2971015.
[134] P. Farago, R. Galatus, M. Cirlugea, S. Hintea, Fluorescent Fiber Implementation of an Angle Sensor, in: 2018 20th Int. Conf. Transparent Opt Networks, IEEE, 2018, pp. 1–4, https://doi.org/10.1109/ICTON.2018.8473637.
[135] R. Galatus, P. Farago, B. Mesesan, S. Hintea, G. Oltean, A. Ilea, Low-Cost Distributed Angle Sensor Implemented on a Fluorescent Fiber, in: 2019 21st Int. Conf. Transparent Opt. Networks, IEEE, 2019, pp. 1–4, https://doi.org/10.1109/ICTON.2019.8840506.
[136] R. Gălătuș, P. Faragó, P. Miluski, J.-A. Valles, Distributed fluorescent optical fiber proximity sensor: Towards a proof of concept, Spectrochim. Acta Part A Mol. Biomol. Spectrosc. 198 (2018) 7–18, https://doi.org/10.1016/j.saa.2018.02.044.
[137] P. Aiestaran, V. Dominguez, J. Arrue, J. Zubia, A fluorescent linear optical fiber position sensor, Opt. Mater. (Amst) 31 (2009) 1101–1104, https://doi.org/10.1016/j.optmat.2007.12.022.
[138] P. Farago, R. Galatus, S. Hintea, J.C. Martín, J. Vallés, Fluorescent fiber implementation of a high-resolution distributed position sensor, in: F. Berghmans, A.G. Mignani (Eds.), Opt. Sens. Detect. V, SPIE, 2018, p. 51, https://doi.org/10.1117/12.2307494.
[139] S. Kamimura, R. Furukawa, Strain sensing based on radiative emission-absorption mechanism using dye-doped polymer optical fiber, Appl. Phys. Lett. 111 (2017), 063301, https://doi.org/10.1063/1.4998738.
[140] J. Guo, B. Zhou, C. Yang, Q. Dai, L. Kong, Stretchable and upconversion-luminescent polymeric optical sensor for wearable multifunctional sensing, Opt. Lett. 44 (2019) 5747, https://doi.org/10.1364/OL.44.005747.
[141] P. Miluski, D. Dorosz, J. Żmojda, M. Kochanowicz, J. Dorosz, Luminescent Polymer Optical Fibre Sensor for Temperature Measurement, Acta Phys. Pol. A 127 (2015) 730–733, https://doi.org/10.12693/APhysPolA.127.730.
[142] J. Guo, B. Zhou, C. Yang, Q. Dai, L. Kong, Stretchable and Temperature-Sensitive Polymer Optical Fibers for Wearable Health Monitoring, Adv. Funct. Mater. 29 (2019) 1902898, https://doi.org/10.1002/adfm.201902898.
[143] P. Farago, A.-M. Băbțan, R. Galatus, R. Groza, N.M. Roman, C.N. Feurdean, A. Ilea, A Side-Polished Fluorescent Fiber Sensor for the Detection of Blood in the Saliva, in: 2019, pp. 23–28. https://doi.org/10.1007/978-981-13-6207-1_4.
[144] Y. He, E. Du, X. Zhou, J. Zhou, Y. He, Y. Ye, J. Wang, B. Tang, X. Wang, Wet-spinning of fluorescent fibers based on gold nanoclusters-loaded alginate for sensing of heavy metal ions and anti-counterfeiting, Spectrochim. Acta Part A Mol. Biomol. Spectrosc. 230 (2020), 118031, https://doi.org/10.1016/j.saa.2020.118031.
[145] R. Inglev, J. Janting, O. Bang, Annular Cavity Design for Photoluminescent Polymer Optical Fiber Sensors, Sensors 20 (2020) 5199, https://doi.org/10.3390/s20185199.
[146] Y. Wang, Y. Zhu, J. Huang, J. Cai, J. Zhu, X. Yang, J. Shen, H. Jiang, C. Li, CsPbBr 3 Perovskite Quantum Dots-Based Monolithic Electrospun Fiber Membrane as an Ultrastable and Ultrasensitive Fluorescent Sensor in Aqueous Medium, J. Phys. Chem. Lett. 7 (2016) 4253–4258, https://doi.org/10.1021/acs.jpclett.6b02045.
[147] M. Hu, W. Kang, Y. Zhao, J. Shi, B. Cheng, A fluorescent and colorimetric sensor based on a porphyrin doped polystyrene nanoporous fiber membrane for HCl gas detection, RSC Adv. 7 (2017) 26849–26856, https://doi.org/10.1039/C7RA02040F.
[148] D. Shu, P. Xi, S. Li, C. Li, X. Wang, B. Cheng, Morphologies and Properties of PET Nano Porous Luminescence Fiber: Oil Absorption and Fluorescence-Indicating Functions, ACS Appl. Mater. Interfaces 10 (2018) 2828–2836, https://doi.org/10.1021/acsami.7b16655.
[149] C.-P. Hsu, Z. Hejazi, E. Armagan, S. Zhao, M. Schmid, H. Zhang, H. Guo, L. Weidenbacher, R.M. Rossi, M.M. Koebel, L.F. Boesel, C. Toncelli, Carbon dots and fluorescein: The ideal FRET pair for the fabrication of a precise and fully reversible ammonia sensor, Sensors Actuators B Chem. 253 (2017) 714–722, https://doi.org/10.1016/j.snb.2017.07.001.
[150] A. Petropoulou, S. Kralj, X. Karagiorgis, I. Savva, E. Loizides, M. Panagi, T. Krasia-Christoforou, C. Riziotis, Multifunctional Gas and pH Fluorescent Sensors Based on Cellulose Acetate Electrospun Fibers Decorated with Rhodamine B-Functionalised Core-Shell Ferrous Nanoparticles, Sci. Rep. 10 (2020) 367, https://doi.org/10.1038/s41598-019-57291-0.
[151] P. Xue, J. Ding, Y. Shen, H. Gao, J. Zhao, J. Sun, R. Lu, Aggregation-induced emission nanofiber as a dual sensor for aromatic amine and acid vapor, J. Mater. Chem. C 5 (2017) 11532–11541, https://doi.org/10.1039/C7TC03192K.
[152] A. Erdman, P. Kulpinski, J. Gabor, A. Stanula, A.S. Swinarew, Luminescent Cellulose Fibers Modified with Poly((9-Carbazolyl)Methylthiirane), Polymers (Basel) 12 (2020) 2296, https://doi.org/10.3390/polym12102296.
[153] P. Miluski, D. Dorosz, M. Kochanowicz, J. Żmojda, Fluorescent polymeric optical fibre illuminator, Electron. Lett. 52 (2016) 1550–1552, https://doi.org/10.1049/el.2016.1491.
[154] N. Cennamo, F. Mattiello, R.V. Galatus, E. Voiculescu, L. Zeni, Plasmonic Sensing in D-Shaped POFs With Fluorescent Optical Fibers as Light Sources, IEEE Trans. Instrum. Meas. 67 (2018) 754–759, https://doi.org/10.1109/TIM.2017.2745018.
[155] C.C. Lin, D.-H. Jiang, C.-C. Kuo, C.-J. Cho, Y.-H. Tsai, T. Satoh, C. Su, Water-Resistant Efficient Stretchable Perovskite-Embedded Fiber Membranes for Light-Emitting Diodes, ACS Appl. Mater. Interfaces 10 (2018) 2210–2215, https://doi.org/10.1021/acsami.7b15989.
[156] L. Jun, G. Qiang, Z. Kaiyan, G. Mingqiao, L. Jialin, Structure and luminescent properties of luminous polypropylene fiber based on Sr2MgSi2O7:Eu2+, Dy3+, J. Rare Earths 32 (2014) 696–701, https://doi.org/10.1016/S1002-0721(14)60128-9.
[157] T. Kobayashi, G. Jordan, W.J. Blau, H. Tillmann, H.-H. Horhold, Luminescent polymer optical fibers: linear and nonlinear spectroscopy and lasing, in: 15th Annu. Meet. IEEE Lasers Electro-Optics Soc., IEEE, n.d.: pp. 265–266. https://doi.org/10.1109/LEOS.2002.1134029.
[158] Z. Hu, Y. Liang, P. Gao, H. Jiang, J. Chen, S. Jiang, K. Xie, Random lasing from dye doped polymer optical fiber containing gold nanoparticles, J. Opt. 17 (2015), 125403, https://doi.org/10.1088/2040-8978/17/12/125403.
[159] Z. Hu, J. Xia, Y. Liang, J. Wen, E. Miao, J. Chen, S. Wu, X. Qian, H. Jiang, K. Xie, Tunable random polymer fiber laser, Opt. Express 25 (2017) 18421, https://doi.org/10.1364/OE.25.018421.
[160] J. He, W.-K. Chan, X. Cheng, M.-L. Tse, C. Lu, P.-K. Wai, S. Savovic, H.-Y. Tam, Experimental and Theoretical Investigation of the Polymer Optical Fiber Random Laser with Resonant Feedback, Adv. Opt. Mater. 6 (2018) 1701187, https://doi.org/10.1002/adom.201701187.
[161] W. Zhu, T. Xu, H. Wang, C. Zhang, P.B. Deotare, A. Agrawal, H.J. Lezec, Surface plasmon polariton laser based on a metallic trench Fabry-Perot resonator, Sci. Adv. 3 (2017), e1700909, https://doi.org/10.1126/sciadv.1700909.
[162] H. Coles, S. Morris, Liquid-crystal lasers, Nat. Photonics 4 (2010) 676–685, https://doi.org/10.1038/nphoton.2010.184.
[163] T. Ali, J. Lin, B. Snow, X. Wang, S.J. Elston, S.M. Morris, Flexible Lasers: A Thin-Film Flexible Defect-Mode Laser (Advanced Optical Materials 8/2020), Adv. Opt. Mater. 8 (2020) 2070034, https://doi.org/10.1002/adom.202070034.
[164] B. Redding, H. Cao, M.A. Choma, Speckle-Free Laser Imaging with Random Laser Illumination, Opt. Photonics News 23 (2012) 30, https://doi.org/10.1364/OPN.23.12.000030.
[165] S.-W. Chang, W.-C. Liao, Y.-M. Liao, H.-I. Lin, H.-Y. Lin, W.-J. Lin, S.-Y. Lin, P. Perumal, G. Haider, C.-T. Tai, K.-C. Shen, C.-H. Chang, Y.-F. Huang, T.-Y. Lin, Y.-F. Chen, A White Random Laser, Sci. Rep. 8 (2018) 2720, https://doi.org/10.1038/s41598-018-21228-w.
[166] B. Redding, M.A. Choma, H. Cao, Speckle-free laser imaging using random laser illumination, Nat. Photonics 6 (2012) 355–359, https://doi.org/10.1038/nphoton.2012.90.
[167] M. Beckers, T. Schlüter, T. Gries, G. Seide, C.A. Bunge, Fabrication techniques for polymer optical fibres, Polym. Opt. Fibres Fibre Types, Mater. Fabr. Characterisation Appl. (2016) 187–199, https://doi.org/10.1016/B978-0-08-100039-7.00006-3.
[168] M. Beckers, T. Schlüter, T. Vad, T. Gries, C.A. Bunge, An overview on fabrication methods for polymer optical fibers, Polym. Int. 64 (2015) 25–36, https://doi.org/10.1002/pi.4805.
[169] J. Guo, X. Liu, N. Jiang, A.K. Yetisen, H. Yuk, C. Yang, A. Khademhosseini, X. Zhao, S.-H. Yun, Highly Stretchable, Strain Sensing Hydrogel Optical Fibers, Adv. Mater. 28 (2016) 10244–10249, https://doi.org/10.1002/adma.201603160.
[170] J. Guo, M. Niu, C. Yang, Highly flexible and stretchable optical strain sensing for human motion detection, Optica 4 (2017) 1285, https://doi.org/10.1364/OPTICA.4.001285.
[171] H. Gao, H. Hu, Y. Zhao, J. Li, M. Lei, Y. Zhang, Highly-sensitive optical fiber temperature sensors based on PDMS/silica hybrid fiber structures, Sensors Actuators A Phys. 284 (2018) 22–27, https://doi.org/10.1016/j.sna.2018.10.011.
[172] M.S. Cano-Velázquez, L.M. López-Marín, J. Hernández-Cordero, Fiber optic biosensor based on polydimethylsiloxane (PDMS) and bioactive lipids, in: I. Gannot (Ed.), Opt. Fibers Sensors Med. Diagnostics Treat. Appl. XX, SPIE, 2020: p. 33. https://doi.org/10.1117/12.2546685.
[173] I. Martincek, D. Pudis, P. Gaso, Polydimethylsiloxane fibers for optical fiber sensor of displacement, in: E.M. Campo, E.A. Dobisz, L.A. Eldada (Eds.), 2013: p. 88161D. https://doi.org/10.1117/12.2024053.
[174] L. Cai, Y. Liu, S. Hu, Q. Liu, Optical fiber temperature sensor based on modal interference in multimode fiber lengthened by a short segment of

polydimethylsiloxane, Microw. Opt. Technol. Lett. 61 (2019) 1656–1660, https://doi.org/10.1002/mop.31843.
[175] O. Sidek, M.H. Bin Afzal, A review paper on fiber-optic sensors and application of PDMS materials for enhanced performance, in: 2011 IEEE Symp. Business, Eng. Ind. Appl., IEEE, 2011, pp. 458–463, https://doi.org/10.1109/ISBEIA.2011.6088858.
[176] C. Jiang, M.G. Kuzyk, J.-L. Ding, W.E. Johns, D.J. Welker, Fabrication and mechanical behavior of dye-doped polymer optical fiber, J. Appl. Phys. 92 (2002) 4–12, https://doi.org/10.1063/1.1481774.
[177] Gang Ding Peng, P.K. Chu, Zhengjun Xiong, T.W. Whitbread, R.P. Chaplin, Dye-doped step-index polymer optical fiber for broadband optical amplification, J. Light. Technol. 14 (1996) 2215–2223, https://doi.org/10.1109/50.541210.
[178] Y. Qu, T. Nguyen-Dang, A.G. Page, W. Yan, T. Das Gupta, G.M. Rotaru, R. M. Rossi, V.D. Favrod, N. Bartolomei, F. Sorin, Superelastic Multimaterial Electronic and Photonic Fibers and Devices via Thermal Drawing, Adv. Mater. 30 (2018) 1707251, https://doi.org/10.1002/adma.201707251.
[179] M. Bayindir, F. Sorin, A.F. Abouraddy, J. Viens, S.D. Hart, J.D. Joannopoulos, Y. Fink, Metal–insulator–semiconductor optoelectronic fibres, Nature 431 (2004) 826–829, https://doi.org/10.1038/nature02937.
[180] W. Yan, Y. Qu, T. Das Gupta, A. Darga, D.T. Nguyên, A.G. Page, M. Rossi, M. Ceriotti, F. Sorin, Semiconducting Nanowire-Based Optoelectronic Fibers, Adv. Mater. 29 (2017) 1700681, https://doi.org/10.1002/adma.201700681.
[181] N.D. Orf, O. Shapira, F. Sorin, S. Danto, M.A. Baldo, J.D. Joannopoulos, Y. Fink, Fiber draw synthesis, Proc. Natl. Acad. Sci. 108 (2011) 4743–4747, https://doi.org/10.1073/pnas.1101160108.
[182] W. Yan, C. Dong, Y. Xiang, S. Jiang, A. Leber, G. Loke, W. Xu, C. Hou, S. Zhou, M. Chen, R. Hu, P.P. Shum, L. Wei, X. Jia, F. Sorin, X. Tao, G. Tao, Thermally drawn advanced functional fibers: New frontier of flexible electronics, Mater. Today 35 (2020) 168–194, https://doi.org/10.1016/j.mattod.2019.11.006.
[183] B. Spear, Let there be light! Sir Joseph Swan and the incandescent light bulb, World Pat. Inf. 35 (2013) 38–41, https://doi.org/10.1016/j.wpi.2012.10.001.
[184] B. Ozipek, H. Karakas, Wet spinning of synthetic polymer fibers, in: Adv. Filam. Yarn Spinn. Text. Polym., Elsevier, 2014, pp. 174–186, https://doi.org/10.1533/9780857099174.2.174.
[185] I.L. Liakos, A. Mondini, C. Filippeschi, V. Mattoli, F. Tramacere, B. Mazzolai, Towards ultra-responsive biodegradable polysaccharide humidity sensors, Mater. Today Chem. 6 (2017) 1–12, https://doi.org/10.1016/j.mtchem.2017.08.001.
[186] A. Grigoryev, V. Sa, V. Gopishetty, I. Tokarev, K.G. Kornev, S. Minko, Wet-Spun Stimuli-Responsive Composite Fibers with Tunable Electrical Conductivity, Adv. Funct. Mater. 23 (2013) 5903–5909, https://doi.org/10.1002/adfm.201203721.
[187] V. Sa, K.G. Kornev, A method for wet spinning of alginate fibers with a high concentration of single-walled carbon nanotubes, Carbon N. Y. 49 (2011) 1859–1868, https://doi.org/10.1016/j.carbon.2011.01.008.
[188] D.H. Reneker, I. Chun, Nanometre diameter fibres of polymer, produced by electrospinning, Nanotechnology 7 (1996) 216–223, https://doi.org/10.1088/0957-4484/7/3/009.
[189] J. Doshi, D.H. Reneker, Electrospinning process and applications of electrospun fibers, J. Electrostat. 35 (1995) 151–160, https://doi.org/10.1016/0304-3886(95)00041-8.
[190] D. Li, Y. Xia, Electrospinning of Nanofibers: Reinventing the Wheel? Adv. Mater. 16 (2004) 1151–1170, https://doi.org/10.1002/adma.200400719.
[191] A.K. Moghe, R. Hufenus, S.M. Hudson, B.S. Gupta, Effect of the addition of a fugitive salt on electrospinnability of poly(ε-caprolactone), Polymer (Guildf) 50 (2009) 3311–3318, https://doi.org/10.1016/j.polymer.2009.04.063.
[192] J.-L. Li, X.-Y. Liu, Architecture of Supramolecular Soft Functional Materials: From Understanding to Micro-/Nanoscale Engineering, Adv. Funct. Mater. 20 (2010) 3196–3216, https://doi.org/10.1002/adfm.201000744.
[193] S.S. Babu, V.K. Praveen, A. Ajayaghosh, Functional π-Gelators and Their Applications, Chem. Rev. 114 (2014) 1973–2129, https://doi.org/10.1021/cr400195e.
[194] Z. Wei, J.H. Yang, J. Zhou, F. Xu, M. Zrínyi, P.H. Dussault, Y. Osada, Y.M. Chen, Self-healing gels based on constitutional dynamic chemistry and their potential applications, Chem. Soc. Rev. 43 (2014) 8114–8131, https://doi.org/10.1039/C4CS00219A.
[195] X. Yu, L. Chen, M. Zhang, T. Yi, Low-molecular-mass gels responding to ultrasound and mechanical stress: towards self-healing materials, Chem. Soc. Rev. 43 (2014) 5346, https://doi.org/10.1039/C4CS00066H.
[196] C.D. Jones, J.W. Steed, Gels with sense: supramolecular materials that respond to heat, light and sound, Chem. Soc. Rev. 45 (2016) 6546–6596, https://doi.org/10.1039/C6CS00435K.
[197] R. Hufenus, Y. Yan, M. Dauner, T. Kikutani, Melt-Spun Fibers for Textile Applications, Materials (Basel) 13 (2020) 4298, https://doi.org/10.3390/ma13194298.
[198] R. Hufenus, Y. Yan, M. Dauner, D. Yao, T. Kikutani, Bicomponent Fibers, in: Handb. Fibrous Mater., Wiley, 2020, pp. 281–313, https://doi.org/10.1002/9783527342587.ch11.
[199] M. Mignanelli, K. Wani, J. Ballato, S. Foulger, P. Brown, Polymer microstructured fibers by one-step extrusion, Opt. Express 15 (2007) 6183, https://doi.org/10.1364/OE.15.006183.
[200] B.-T. Liu, W.-C. Chen, J.-P. Hsu, Mathematical modeling of a co-extrusion process for preparing gradient-index polymer optical fibers, Polymer (Guildf) 40 (1999) 1451–1457, https://doi.org/10.1016/S0032-3861(98)00387-5.
[201] J.-P. Hsu, S.-H. Lin, Analysis of co-extrusion process for preparation of gradient index plastic optical fiber, Polymer (Guildf) 44 (2003) 5461–5467, https://doi.org/10.1016/S0032-3861(03)00575-5.
[202] R. Hirose, M. Asai, A. Kondo, Y. Koike, Preparation of graded-index plastic optical fiber by co-extrusion process, in: J.G. Grote, F. Kajzar, N. Kim (Eds.), 2007, p. 64700K. https://doi.org/10.1117/12.700193.
[203] R. Hufenus, L. Gottardo, A.A. Leal, A. Zemp, K. Heutschi, P. Schuetz, V.R. Meyer, M. Heuberger, Melt-spun polymer fibers with liquid core exhibit enhanced mechanical damping, Mater. Des. 110 (2016) 685–692, https://doi.org/10.1016/j.matdes.2016.08.042.
[204] A.A. Leal, M. Naeimirad, L. Gottardo, P. Schuetz, A. Zadhoush, R. Hufenus, Microfluidic behavior in melt-spun hollow and liquid core fibers, Int. J. Polym. Mater. Polym. Biomater. 65 (2016) 451–456, https://doi.org/10.1080/00914037.2015.1129957.
[205] B.M. Quandt, M.S. Pfister, J.F. Lübben, F. Spano, R.M. Rossi, G.-L. Bona, L. F. Boesel, POF-yarn weaves: controlling the light out-coupling of wearable phototherapy devices, Biomed. Opt. Express 8 (2017) 4316, https://doi.org/10.1364/BOE.8.004316.
[206] M. Beckers, T. Vad, B. Mohr, B. Weise, W. Steinmann, T. Gries, G. Seide, E. Kentzinger, C.A. Bunge, Novel melt-spun polymer-optical poly(methyl methacrylate) fibers studied by small-angle X-ray scattering, Polymers (Basel) 9 (2017), https://doi.org/10.3390/polym9020060.
[207] C.-A. Bunge, M. Beckers, T. Gries, Simple and adjustable fabrication process for graded-index polymer optical fibers with tailored properties for sensing, in: IEEE SENSORS 2014 Proc., 2014, pp. 1527–1530, https://doi.org/10.1109/ICSENS.2014.6985306.
[208] B. Lustermann, B.M. Quandt, S. Ulrich, F. Spano, R.M. Rossi, L.F. Boesel, Experimental determination and ray-tracing simulation of bending losses in melt-spun polymer optical fibres, Sci. Rep. 10 (2020) 11885, https://doi.org/10.1038/s41598-020-68568-0.
[209] Dopant-free fabrication process for graded-index polymer optical fiber solely based on temperature treatment, in: 2015 17th Int. Conf. Transparent Opt. Networks, IEEE, 2015: pp. 1–4. https://doi.org/10.1109/ICTON.2015.7193647.
[210] J. Kallweit, C.-A. Bunge, T. Vad, T. Gries, Systematic investigation of a modified melt spinning manufacturing parameters on the structural properties of graded index polymer optical fibers, in: C.-A. Bunge, K. Kalli, P. Peterka (Eds.), Micro-Structured Spec. Opt. Fibres VI, SPIE, 2020, p. 5, https://doi.org/10.1117/12.2563901.
[211] C.-A. Bunge, B. Mohr, T. Vad, M. Beckers, T. Gries, Fabrication and analysis of side-emitting poly(methyl methacrylate) fibres with non-circular cross-sections, Polym. Int. 67 (2018) 1170–1178, https://doi.org/10.1002/pi.5605.